

STRATIGRAPHY, SEDIMENTARY STRUCTURES, AND TEXTURES OF THE LATE NEOPROTEROZOIC DOUSHANTUO CAP CARBONATE IN SOUTH CHINA

GANQING JIANG,¹ MARTIN J. KENNEDY,² NICHOLAS CHRISTIE-BLICK,³ HUAICHUN WU,⁴ AND SHIHONG ZHANG⁴

¹Department of Geoscience, University of Nevada, Las Vegas, Nevada 89154-4010, U.S.A.

²Department of Earth Sciences, University of California, Riverside, California 92521, U.S.A.

³Department of Earth and Environmental Sciences and Lamont-Doherty Earth Observatory of Columbia University, Palisades, New York 10964-8000, U.S.A.

⁴School of Earth Sciences and Resources, China University of Geosciences, Beijing 100083, China

e-mail: jiangg@unlv.nevada.edu

ABSTRACT: The 3- to 5-m-thick Doushantuo cap carbonate in south China overlies the glaciogenic Nantuo Formation (ca. 635 Ma) and consists of laterally persistent, thinly laminated and normally graded dolomite and limestone indicative of relatively deep-water deposition, most likely below storm wave base. The basal portion of this carbonate contains a distinctive suite of closely associated tepee-like structures, stromatactis-like cavities, layer-parallel sheet cracks, and cemented breccias. The cores of tepees are composed of stacked cavities lined by cements and brecciated host dolomicrite. Onlap by laminated sediment indicates syndepositional disruption of bedding that resulted in a positive seafloor expression. Cavities and sheet cracks contain internal sediments, and they are lined by originally aragonitic isopachous botryoidal cements with acicular radiating needles, now replaced by dolomite and silica. Pyrite and barite are common, and calcite is locally retained as a primary mineral. These features share morphological and petrographic attributes with modern and ancient methane seeps in which methane gas and fluids provide both a force for physical disruption from buoyancy and a source of alkalinity for significant cementation. The presence of $\delta^{13}\text{C}$ values as low as -41% in well preserved limestone crusts and cements within and immediately above the tepee-like structures provides unequivocal evidence for methane influence, and the widespread distribution of identical sedimentary structures and paragenetic cement sequences across the entire basin at the same basal carbonate level is consistent with gas hydrate destabilization and the development of methane seeps as a result of postglacial warming of the ocean. Considering the broad distribution of similar features at the same stratigraphic level in other cap carbonates globally, we suggest that the late Neoproterozoic postglacial methane release may have influenced the oceanic oxygen level as well as contributed to postglacial warming via the greenhouse effects of methane.

INTRODUCTION

One of the most puzzling phenomena of the late Neoproterozoic from ~ 750 Ma to 543 Ma is the global occurrence of thin “cap carbonates” that in many places directly overlie glacial deposits and produce unusual carbon isotope values from $+1\%$ to -9% (e.g., Kennedy 1996; Kaufman et al. 1997; Hoffman et al. 1998; Kennedy et al. 1998; James et al. 2001; Kennedy et al. 2001; Hoffman and Schrag 2002; Leather et al. 2002; Jiang et al. 2003a; Nogueira et al. 2003; de Alvarenga et al. 2004; Halverson et al. 2004; Porter et al. 2004; Xiao et al. 2004; Zhou et al. 2004), with a few examples yielding $\delta^{13}\text{C}$ values as low as -10% (Xiao et al. 2004; Halverson et al. 2004) to -41% (Jiang et al. 2003a). The origin of these deposits remains controversial, with three ideas dominating current thinking: (1) the snowball Earth hypothesis, in which the cap carbonate represents the transfer of CO_2 from the atmospheric to the sedimentary reservoir via silicate and carbonate weathering (Hoffman et al. 1998; Hoffman and Schrag 2002; Higgins and Schrag 2003); (2) the upwelling model, in which physical stratification produces a strong surface-to-deep carbon isotope gradient in the ocean, and postglacial upwelling or flooding delivers alkalinity-rich deep water to continental shelves and interior basins, resulting in carbonate precipitation (Grotzinger and Knoll 1995; Knoll et al. 1996; Kaufman et al. 1997; Ridgwell et al. 2003; Shields

2005); and (3) the methane hypothesis, in which the cap carbonates and associated isotopic anomaly are due to methane oxidation in a supersaturated ocean following a time of extreme cold (Kennedy et al. 2001; Jiang et al. 2003a).

Cap carbonates globally have three attributes: (1) a nearly universal distribution and relatively uniform thickness of 1 to 10 m over glacially related sediments, (2) a comparable negative carbon isotope signature (with $\delta^{13}\text{C}$ values that decline to $< -5\%$) at widely separated locations, and (3) an unusual suite of sedimentary structures and textures, including tepee-like structures, stromatactis-like cavities, sheet cracks, cemented breccias, tube structures, and barite fans, which are sporadically distributed in almost all documented cap carbonates (e.g., Deynoux et al. 1976; Plummer 1978; Williams 1979; Walter and Bauld 1983; Aitken 1991; Kennedy 1996; Kennedy et al. 1998; James et al. 2001; Kennedy et al. 2001; Hoffman and Schrag 2002; Leather et al. 2002; Jiang et al. 2003a; Nogueira et al. 2003; de Alvarenga et al. 2004; Halverson et al. 2004; Porter et al. 2004; Xiao et al. 2004; Zhou et al. 2004; Allen and Hoffman 2005). Most discussions have focused on the overall distribution and carbon isotope characteristics of the carbonates, which have been taken to imply a major chemical oceanographic event in the aftermath of glaciation. Rather less attention has been paid to the processes

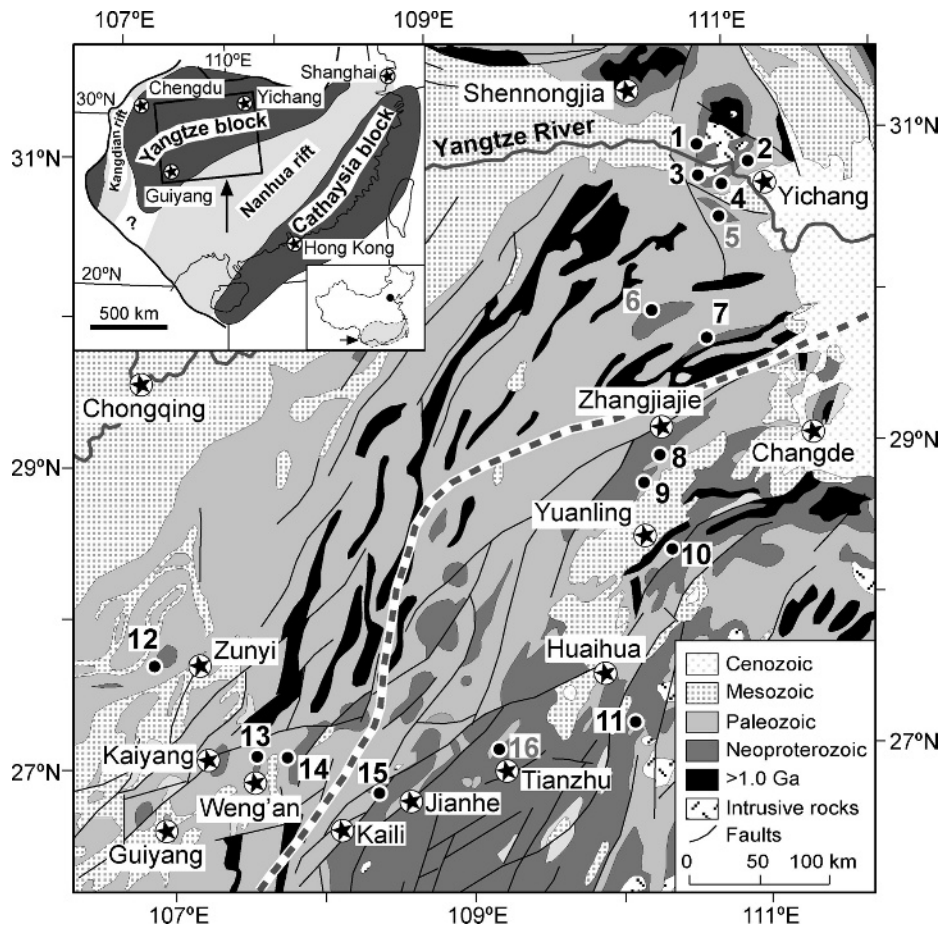


FIG. 1.—Simplified geological map showing exposures of Neoproterozoic strata in the Yangtze platform of south China and position of the late Proterozoic platform margin (coarse dotted line). The top left inset shows the Neoproterozoic tectonic framework, emphasizing the inferred continental rift systems at ca. 800 Ma (see Jiang et al. 2003b for details). Black numbers indicate location of measured cap carbonate sections (Figs. 3–5): 1 = Miaohe; 2 = Liantuo; 3 = Jiuqunao; 4 = Huajipo; 7 = Yangjiaping; 8 = Tianping; 9 = Siduping; 10 = Fengtan; 11 = Yuanjia; 12 = Songling; 13 = Wen'an; 14 = Duoding; 15 = Wuhe. Sections 4A and B (Fig. 4) are about 500 m apart in the same locality.

responsible for the unusual sedimentary structures and textures (e.g., Kennedy 1996; James et al. 2001; Kennedy et al. 2001; Jiang et al. 2003a; Nogueira et al. 2003; Allen and Hoffman 2005; Gammon et al. 2005), although the appearance of these features has been mentioned in every recent publication related to the cap carbonates, underscoring their universality in these deposits.

Early interpretations ascribed the tepee-like structures in the Nuccaleena Formation of South Australia to supratidal processes (e.g., Plummer 1978; Williams 1979), although a relatively deep-water origin for these and most other cap carbonates is now widely accepted (Kennedy 1996; Hoffman and Schrag 2000). Sheet cracks and tubes observed in the Noonday Dolomite of eastern California and in the Bildah Formation of southern Namibia were suggested to be gas-escape features (Cloud et al. 1974; Hegenberger 1987), possibly caused by CO_2 release from photosynthetic mats. Other interpretations suggested for tepee-like structures in cap carbonates include (1) syndepositional deformation and cementation (e.g., Kennedy 1996; James et al. 2001); (2) seismicity-related deformation (e.g., Nogueira et al. 2003); (3) giant wave ripples (Allen and Hoffman 2005); and (4) seafloor dolomite cementation during early diagenesis (e.g., Plummer 1978; Gammon et al. 2005; Shields 2005). While these mechanisms may account for specific features in cap carbonates at individual locations, none accounts for the full suite of structures and textures involving synsedimentary buckling and cementation, their broad distribution, and stratigraphic restriction within the lower portion of all cap carbonates.

In contrast, Kennedy et al. (2001) and Jiang et al. (2003a) proposed that the tepee-like structures, sheet cracks, tube structures, barite fans, negative carbon isotope values, and associated cavities in Australia,

Namibia, eastern California, and south China were caused by escape of gas and fluid associated with gas-hydrate destabilization triggered by marine transgression and warming after a time of extreme cold. Methane gas liberated from hydrates resulted in localized deformational features around seep pathways, and microbial oxidation led to the precipitation of secondary carbonates.

No detailed documentation of the temporal and spatial variation of these sedimentary structures and textures is currently available at a basin scale, but such data are important for understanding the origin and significance of these features and their role in cap-carbonate deposition in general. The Doushantuo cap carbonate overlying the glaciogenic Nantuo Formation in south China is one of the best preserved Marinoan-age cap carbonates (Jiang et al. 2003a; Zhou et al. 2004) and is traceable with consistent lithology and internal stratigraphy for at least 350 km in platform-to-basin transects (Figs. 1, 2). The purpose of this article is to document and interpret the stratigraphy and sedimentary features of this cap carbonate and to discuss implications for alternative postglacial paleoceanographic models.

GEOLOGICAL BACKGROUND

Tectonic History

A Neoproterozoic rifted continental margin is inferred to have developed along the southeastern side of the Yangtze block after about 800 Ma (Fig. 1; Wang et al. 1985; Liu et al. 1991; Li et al. 1999; Jiang et al. 2003b; Ling et al. 2003; Wang and Li 2003). The precise timing of the rift to post-rift transition is still debatable (Jiang et al. 2003b; Wang and Li 2003; Zheng 2003; Zheng et al. 2004) but is tentatively interpreted to

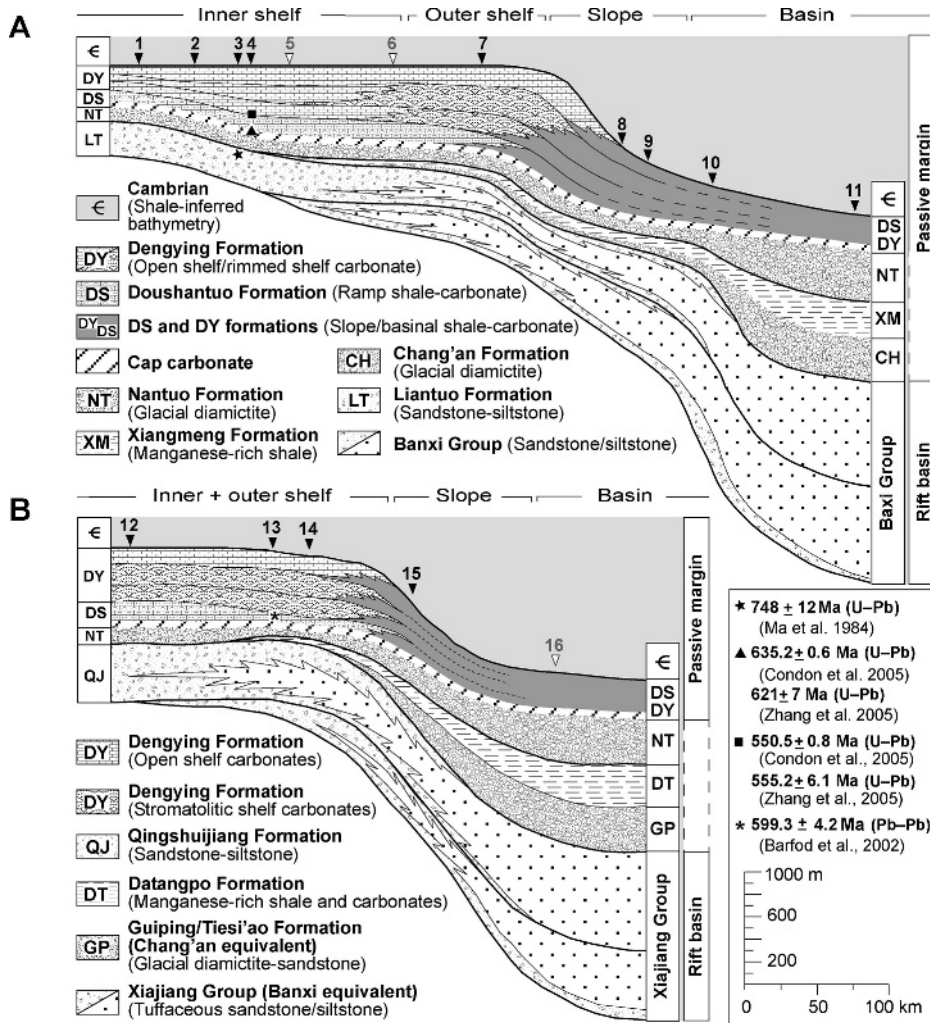


FIG. 2.—The Neoproterozoic platform-basin transects in south China showing the stratigraphic occurrence of the Doushantuo cap carbonates. **A**) Platform-to-basin transect 1 from north to south. **B**) Platform-to-basin transect 2 from west to east. Section numbers match those in Figure 1.

correspond with a level within or at the base of the lower glaciogenic unit (Fig. 2). A passive-margin setting has been inferred for postglacial carbonate rocks, on the basis of platform scale, comparatively simple physical stratigraphic and facies architecture, and the thickness of the succession, with no evidence for either syndepositional tectonism or significant igneous activity (Jiang et al. 2003b), although with unresolved questions about an apparent increase in the rate of subsidence in the latest Neoproterozoic (~ 550 Ma; Fig. 2A) and the lengthy span of time represented. Carbonate deposition continued through Cambrian to middle Ordovician time and ended with Silurian orogeny, during which the Neoproterozoic-lower Paleozoic strata were deformed (Liu et al. 1993). From the late Silurian to early Devonian, much of the South China Block (SCB) was exposed and subjected to weathering and erosion. Subsequent rifting and subsidence, beginning in the middle to late Devonian along the western to southwestern and southeastern sides of the SCB, led to the accumulation of shallow marine clastic and carbonate deposits of late Devonian to middle Triassic age (Wang et al. 1985; Liu et al. 1993). Mesozoic to Cenozoic orogeny associated with the amalgamation of North and South China blocks, the collision between Lhasa and South China blocks, and possibly the subduction of the Pacific plate beneath eastern Asia (Yin and Nie 1996) led to the uplift of the entire SCB, creating much of the exposure seen today. The maximum burial depth of the Neoproterozoic carbonate rocks prior to Silurian orogeny was about 4 km for the platformal deposits and 7 km for those accumulating in the basin. Subsequent burial from Devonian to

Cretaceous was localized and mostly limited, except in the Sichuan basin to the immediate northwest of the study area (Fig. 1). There, Mesozoic and Cenozoic strata are more than 6 km thick.

Stratigraphy and Geochronology

The Neoproterozoic succession of the Yangtze block begins at the base with the Banxi and Xiajiang groups and their equivalents (Fig. 2; Wang et al. 1985; Qiao 1989; Liu et al. 1991; Liu et al. 1993). At the southeastern margin of the block, these units are composed of > 2 km of deep-marine turbidites and volcanic rocks; the nonmarine equivalent in the interior of the Yangtze block (Liantuo Formation in Hubei, Fig. 2A; and Qingshuijiang or Liangjiehe formations in Guizhou, Fig. 2B) is thin (< 500 m). Ash beds within the upper part of the Banxi Group and Liantuo Formation yield U-Pb zircon ages of 758 ± 23 Ma and 748 ± 12 Ma (Ma et al. 1984; Zhao et al. 1985; Yin et al. 2003), respectively. Unconformably overlying these rocks are glacial sediments of the Chang'an Formation (Gucheng Formation in Hubei, Fig. 2A; Guiping and Tiesi'ao formations in Guizhou, Fig. 2B; but see Zhou et al. 2004 for a different view), commonly interpreted to be of Sturtian age ($< \sim 720$ Ma). The Chang'an Formation is overlain by carbonaceous, manganese-bearing siltstone and shale of the Datangpo Formation. Patchy limestone and dolomite lenses and carbonate concretions present in the lower to middle Datangpo Formation have been plausibly regarded as the cap carbonate of the lower glacial diamictite (Zhou et al. 2001). A

U–Pb age of 663 ± 4 Ma for a tuffaceous bed at the base of the Datangpo Formation (Zhou et al. 2004) provides an upper age constraint for this lower glacial interval. The Datangpo Formation is overlain by glaciogenic rocks of the Nantuo Formation, which is overlain in turn by a thin (< 5 m) cap carbonate dated at 635.2 ± 0.6 Ma (Condon et al. 2005) and 621 ± 7 Ma (Zhang et al. 2005), respectively. The Nantuo Formation and correlative units are typically thin in the interior of the Yangtze block (~ 100 m), but they thicken markedly towards the southeast (< 4 km; Jiang et al. 2003b), a trend that is consistent with that of the preglacial strata. In contrast, postglacial marine carbonate and shale (Doushantuo and Dengying formations) thin from as much as 1,000 m in the interior of the Yangtze block to < 250 m of siliceous shale and carbonate in the adjacent basin (Fig. 2). The Doushantuo Formation contains two phosphorite-bearing units from which abundant embryos that are arguably ascribed to animal fossils (e.g., Xiao et al. 1998; Yin et al. 2004), multicellular algae, and giant process-bearing, acanthomorph acritarchs have been recovered (Zhang et al. 1998; Yin 1999; Xiao 2004). Pb–Pb ages of 599 ± 4 Ma (Barfod et al. 2002) and 576 ± 14 Ma (Chen et al. 2004) have been reported from these phosphorites. Ediacaran body fossils and trace fossils have been reported from the Dengying Formation (Sun 1986; Zhao et al. 1988; Steiner et al. 1993; Xiao et al. 2005). The transition between the Doushantuo and Dengying formations has been dated as 550.5 ± 0.8 Ma (Condon et al. 2005) and 555.2 ± 6.1 Ma (Zhang et al. 2005). Interstratified carbonate, argillite, chert, and phosphorite of Cambrian age are highly condensed. The basal Cambrian contains small shelly fossils, and has been dated as $< 539 \pm 34$ Ma (Compston et al. 1992), broadly consistent with an age of 542 Ma for the Precambrian–Cambrian boundary (Grotzinger et al. 1995; Bowring and Erwin 1998; Amthor et al. 2003).

Paleogeographic Constraints

Our paleogeographic reconstruction of a southeast-facing late Neoproterozoic Yangtze platform (Figs. 1, 2) is based on two lines of evidence. First, glaciogenic diamictite units underlying the Doushantuo cap carbonate thicken in that direction (Fig. 2; Jiang et al. 2003b), from < 100 m in the shelf (sections 1–7 and 12–14; Fig. 2) to > 1000 m in the inferred basin (e.g., section 11, Fig. 2 and still farther south; Jiang et al. 1996). Second, the postglacial siliciclastic–carbonate succession (Doushantuo and Dengying formations) is characterized by clear evidence for a platform edge. In transect 1, an outer-platform stromatolite-rich shoal complex (cf. Jiang et al. 2003c) thins basinward and changes facies both basinward and into lagoonal deposits of the platform interior (sections 6 and 7 in Fig. 2A; Jiang et al. 2003b). A marginal shoal complex is less well defined in transect 2 (Fig. 2B), where stromatolite-bearing peritidal carbonates in the upper part of the Doushantuo Formation and throughout the Dengying Formation suggest an open shelf. Slump blocks, olistostrome breccias, and turbidites are abundant in both units in sections 8 and 9 of transect 1 and section 15 of transect 2 (Fig. 2), and at other locations along the inferred platform margin (Fig. 1).

STRATIGRAPHY, SEDIMENTARY STRUCTURES, AND TEXTURES OF THE DOUSHANTUO CAP CARBONATE

Stratigraphy

The 3–5-m-thick cap carbonate forming the base of the Doushantuo Formation contains three lithologically distinguishable but laterally variable carbonate units (Figs. 3–6; Jiang et al. 2003a): a basal strongly disrupted and cemented layer (C1), 1–1.9 m thick, a middle laminated layer, less than 2 m thick, with local tepee-like structures (C2), and an upper thinly laminated silty and shaly limestone and dolomite (C3), 1–2 m thick. The predominant lithology of these units is microcrystalline

dolomite and dolomicrite, with sparry calcite, dolomite, and quartz filling crosscutting fractures. Thin and laterally discontinuous (commonly < 5 cm) limestone (micrite) intervals are preserved only locally in platform sections (sections 1–7 in Figs. 1 and 2).

The contact with the underlying Nantuo Formation is a well-exposed, abrupt lithic change in all of the sections examined (Figs. 3–6). This contact was previously interpreted as a disconformity or sequence boundary (Wang et al. 1981; Wang et al. 1998), implying no genetic relation between the glacial event and deposition of the cap carbonate. Our more recent observations lead us to suspect a relatively continuous transition at the end of glaciation involving inundation of the terrigenous source and a switch from proximal glacial-marine sediments of the Nantuo Formation to distal hemipelagic sedimentation within the basal Doushantuo Formation. Evidence includes (1) the presence in the basal 0.5 m of the carbonate of $< 30\%$ siliciclastic components compositionally identical to the matrix of the underlying diamictite; and (2) the absence of evidence for subaerial exposure, channel incision, or nonmarine sedimentation at the contact, independent of paleogeographic location (Fig. 6). The cap carbonate is thus inferred to represent overall deepening of the depositional environment that presumably began during the glacial retreat responsible for deposition of the Nantuo Formation.

The basal carbonate unit (C1) is the most distinctive, consisting of cliff-forming, buff- to yellow-weathering microcrystalline dolomite that is commonly brecciated and associated with cavities lined by multiple generations of fringing cements (Figs. 3–6). Localized limestone blocks are preserved locally in the platform sections (sections 1–5 in Figs. 1, 2), and they change both vertically and laterally into dolomitic limestone and dolomite. The abundance of bedding disruption, brecciation and cementation varies laterally over a few meters to hundreds of meters between three end member types: (1) strongly disrupted and brecciated carbonate, with stromatolite-like cavities, tepee-like structures, sheet cracks, and cements accounting for $< 30\%$ of the bulk rock (see below); (2) less disrupted carbonate with $< 10\%$ composed of cements filling fractures and stromatolite-like cavities; and (3) undisrupted, laminated carbonate. Although localized, highly disrupted facies are present in most of the sections measured from the platform to basin. Comparable cavities and cements have been observed in coeval cap carbonates in Australia (Kennedy 1996), Namibia (Hegenberger 1987; Kennedy et al. 2001), eastern California (Cloud et al. 1974), and Norway (Siedlecka and Roberts 1992).

The change from the basal unit (C1) to the overlying laminated dolomite unit (C2) is transitional, with a decrease of cavity-filling cements and an increase in the continuity of laminae. The basal layers of this unit are locally disrupted by tepee-like structures. Overlying laminated dolomites onlap and thin across the crests of these structures, which are inferred on this basis to have been topographic features at the seafloor. Unit C2 has been recognized in both platform and slope sections but not in inferred basinal sections where unit C1 is overlain directly by shaly dolomite (e.g., Fig. 4F, G).

Unit C2 is transitional to a thinly laminated, silty and shaly dolomite and limestone (unit C3). This unit is the most variable in both thickness and lithology. In platform facies of the Yangtze gorge area (Figs. 3, 4A, B), it is composed predominantly of peloidal dolopackstone, dolowackestone, and dolomicrite containing $< 30\%$ quartz silt, but with only minor shale. To the south in outer-shelf, slope, and basinal sections (Fig. 4C–G), it is characterized by shaly dolomite. In contrast, in the platform-to-slope transect in Guizhou (Fig. 5) this unit is indistinguishable from unit C2 in most places. The contact with the overlying black shale and limestone or dolomite (unit D) is transitional, with a gradual increase in shale. There is no evidence for erosion or subaerial exposure along this contact.

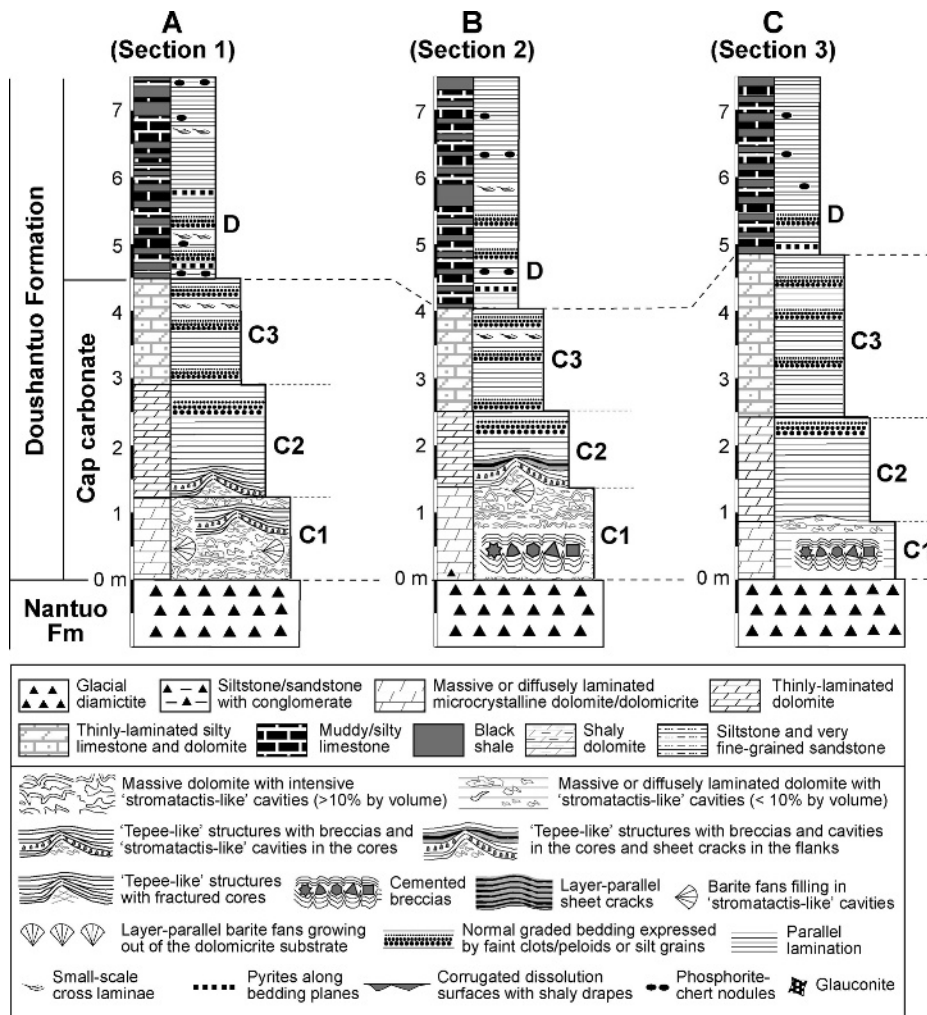


FIG. 3.—Representative Doushantuo cap carbonate sections from the platform setting in transect 1 (Fig. 2A). See Figures 1 and 2 for location of sections.

Sedimentary Structures and Textures

Particles and Lamination.—Microcrystalline dolomite and dolomicrite, the most pervasive phase of the Doushantuo cap carbonate (80% by volume), is composed of microcrystals from 5 to 25 μm in diameter and is characterized by dull to orange luminescence. Dolomite crystals ranging from 30 to 100 μm overgrow the groundmass, with some dolomite rhombs in the matrix, fractures, and cavities exceeding 500 μm .

The dolomicrite matrix surrounds ghosts of clots (0.2–2 mm) and peloids (50–200 μm). Indefinite margins (Fig. 7A, B) indicate partial recrystallization and progressive but incomplete replacement. Euhedral pyrite crystals from 10 to 50 μm in diameter dissimulate the matrix and form thin layers along bedding planes. Pyrite layers are more abundant in outer-shelf to basinal sections than in platform sections (Figs. 3–5). Framboidal pyrite clusters 5 to 15 μm across are evident in scanning electron microscope (SEM) images of clots and peloids (Jiang et al. 2003a). Up to 30% of terrigenous quartz silt is present in the basal 0.5 m of the cap carbonate in all of the measured sections and within unit C3 in the platform sections (Figs. 3, 4A, B).

The basal unit (C1) lacks obvious laminae, owing to recrystallization, bedding disruption, brecciation, and cementation. Only in the least disrupted regions are cryptic laminae 3–5 mm thick occasionally preserved in the form of normally graded peloids or quartz silt or sand particles. In contrast, parallel lamination (Fig. 7C) is common in units C2 to D, where it is expressed by carbonate laminae 1–10 mm thick separated

by dark, pyrite-rich clay-rich drapes < 1 mm thick. Normally graded layers 1–3 mm thick, and consisting of faint clots and peloids (Fig. 7B), and quartz sand or silt, are present from the upper part of C2 to D in most sections measured (Figs. 3–5). In platform sections (e.g., Figs. 3A, B, 4A, 5A–C), asymmetric ripple cross-lamination (Fig. 7D) is present in units C3 and D. In slope to basinal sections (e.g., Fig. 4C, D), unit C3 and D contain corrugated dissolution surfaces at shale–dolomite contacts. Clay-rich drapes up to 1–4 cm thick filling depressions at these dissolution surfaces are overlapped by shale or dolomicrite laminae and are inferred to be of primary origin, similar to those described from the coeval cap carbonates in Australia (Kennedy 1996). Abundant pyrite grains are found along these surfaces.

Stromatactis-Like Cavities.—Stromatactis-like cavities are the most characteristic feature of the basal Doushantuo cap carbonate (unit C1 and lower C2). They are present in all sections in platform-to-basin transects (Figs. 3–5). Individual cavities vary from 0.5 to 5 cm across, and they are commonly connected by fractures to form a reticulate pattern (Fig. 8A). Cavities have low profiles in a continuum with layer-parallel sheet cracks at the base of the cap carbonate (Fig. 8A). These features are focused, and they form additional space within the cores of the tepee-like structures, where they show increasingly higher profile upward in the cores and laterally connecting to low-profile sheet cracks away from the tepee-like structures (Fig. 8B). Unlike typical stromatactis of Paleozoic mud mounds, in which cavities commonly have flat to undulose smooth

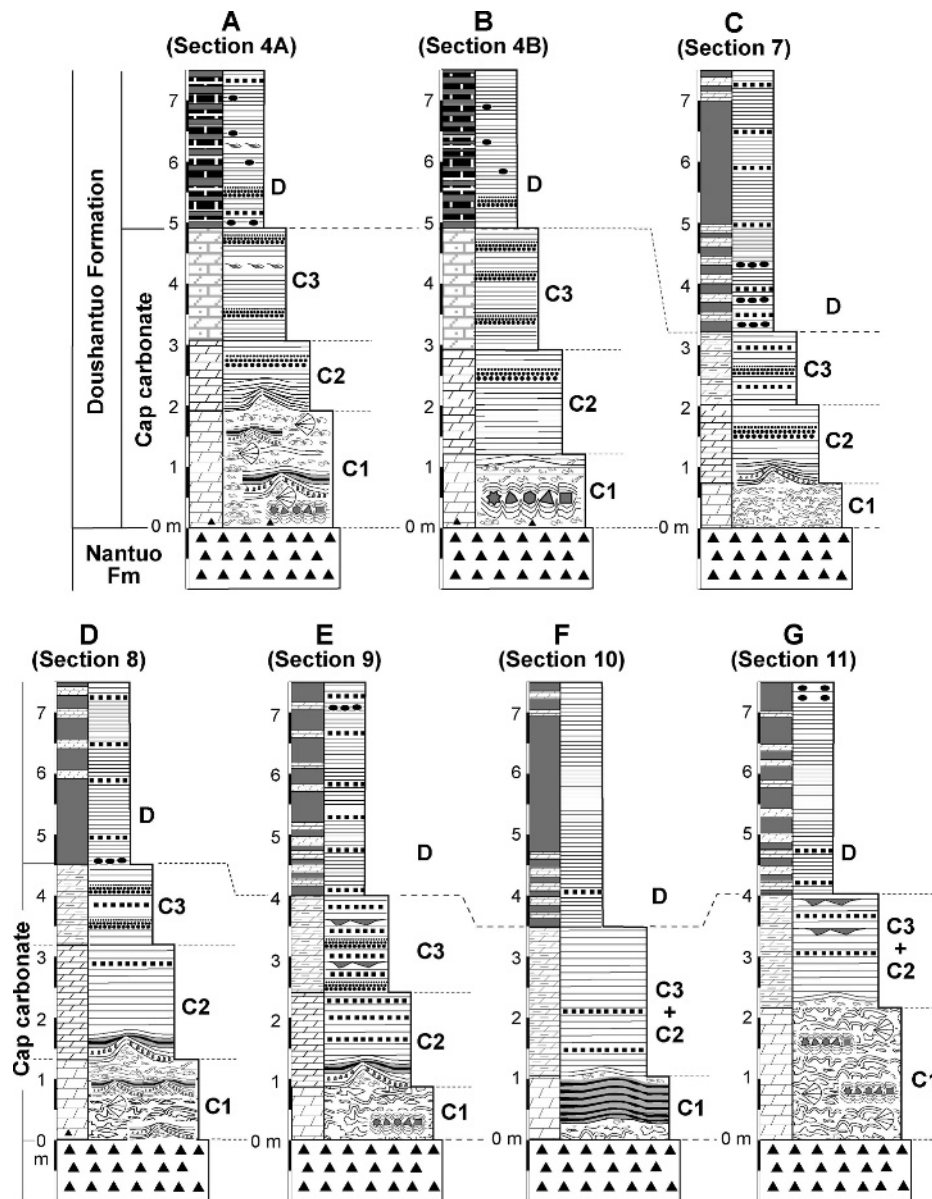


FIG. 4.—Representative sections of the Doushantuo cap carbonate from platform-to-basin settings in transect 1 (Fig. 2A). See Figures 1 and 2 for location of sections and Figure 3 for legends.

lower surfaces and convex upper surfaces (e.g., Wallace 1987; Bourque and Boulvain 1993; Hladil 2005), stromatactis-like cavities of the Doushantuo cap carbonate are characterized either by corrugated upper and lower surfaces (Fig. 8A) or by a relatively flat upper surface (Fig. 9A). The latter is similar to the “inverted stromatactoid” cavities described by Peckmann et al. (2002) and Peckmann and Thiel (2004) from modern and ancient methane seeps and the “gas blisters” in the Noonday Dolomite (Cloud et al. 1974).

Well-preserved stromatactis-like cavities are commonly filled with the following components (e.g., Fig. 9A–C): (1) internal sediment (IS) composed of microcrystalline dolomite and fine-grained quartz silt; (2) isopachous botryoidal cements (IB) consisting of aggregates of very fine acicular needles (1–5 μm) that form either botryoids with 0.4–1.5 mm radius or thin (0.1–0.5 mm) layers; and (3) equant calcite (EC) and dolospar (ED). The splayed or bladed crystal terminations of isopachous botryoidal cements (Fig. 9B, C) are characteristic of aragonite (e.g., Sandberg 1985; James and Choquette 1990; Tucker et al. 1990; Savard et al. 1996). In some cases, isopachous columnar fibrous cements (IC)

nucleate directly on dolomitic matrix, with individual crystal fans up to 2 cm across (Fig. 9D), similar in shape and crystal termination to the radial fibrous calcites described by Kendall and Tucker (1973) and Kendall (1985) from Paleozoic reefs and mud mounds.

Internal sediments both overlie isopachous cement and are overlain by isopachous botryoidal cement fringes. The interbedding of cavity-lining cement and internal sediment requires that these features formed when the cavities were open to the seafloor and sediments could be washed in, and they remained open long enough to be filled by cavity-lining cements (Fig. 9).

Most stromatactis-like cavities are now filled with silica, or secondary carbonate composed of baroque dolomite or sparry calcite. Carbonate textures within pervasively silicified cavity fills are no longer preserved. Silica-filled cavities are commonly connected by quartz-filled crosscutting veins, suggesting that silicification occurred during a later phase of diagenesis. This is consistent with the association of baroque dolomite (e.g., Moore 1989) and the depleted $\delta^{18}\text{O}$ values in both silica ($\leq -15\%$, PDB; Chu Xuelei, personal communication 2005) and calcite and

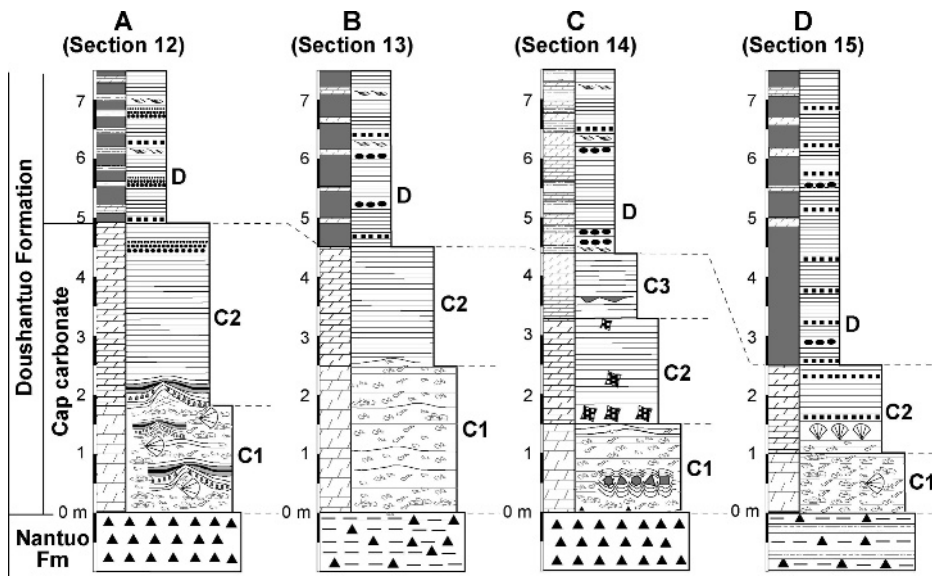


FIG. 5.—Representative sections of the Doushantuo cap carbonate from platform-to-slope settings in transect 2 (Fig. 2B). See Figures 1 and 2 for location of sections and Figure 3 for legends.

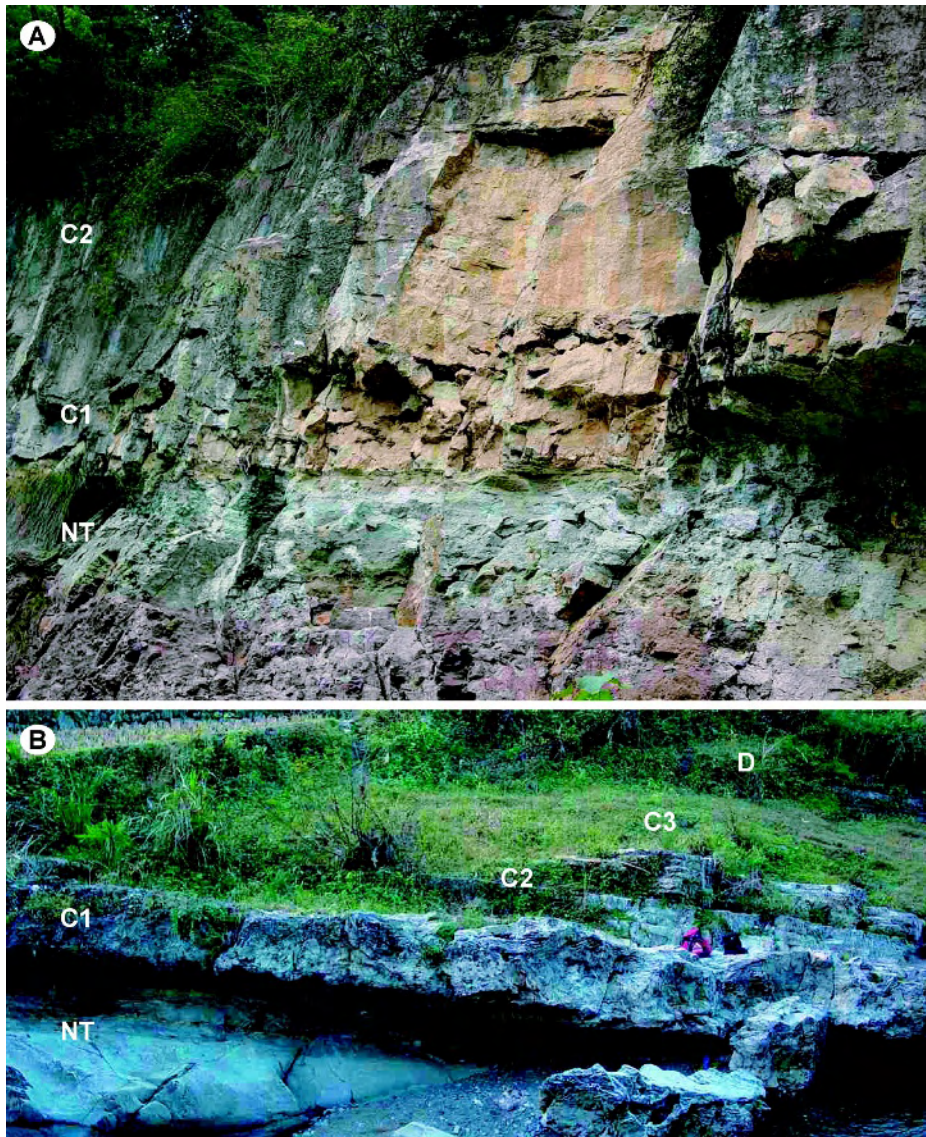


FIG. 6.—Sharp contact between the Doushantuo cap carbonate and the underlying glaciogenic Nantuo Formation (NT), and cap carbonate stratigraphy. A) From Liantuo section (Fig. 3B) in interpreted platform setting; B) from Tianping section (Fig. 4D) in interpreted slope setting. Units C1 to D are the same as those in Figures 3B and 4D.

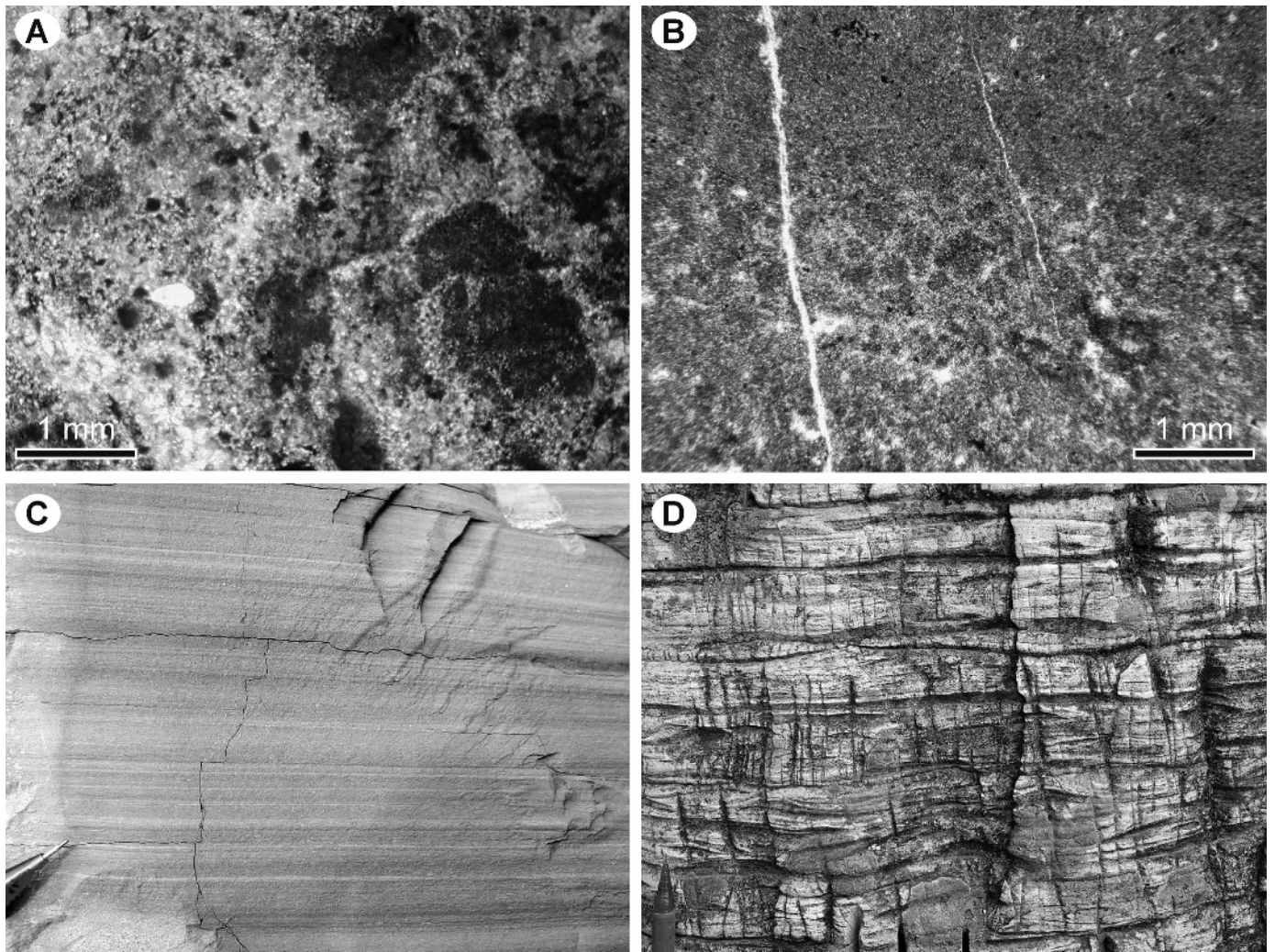


FIG. 7.—Particles and laminae of the Doushantuo cap carbonate. **A)** Clotted dolopackstone showing normally graded bedding. **B)** Peloidal dolopackstone showing normally graded bedding. **C)** Peloidal dolopackstone and dolomicrite showing millimeter-scale parallel lamination and normally graded bedding. **D)** Peloidal dolopackstone showing small-scale cross lamination. A and B are from unit C2 in Figure 4B; C and D are from unit C3 in Figure 4A.

dolomite spars (e.g., points 19 and 20 in Fig. 10; $\delta^{18}\text{O}$ values $\leq -14\%$, PDB).

Tepee-Like Structures.—Tepee-like structures present in the basal Doushantuo cap carbonate (C1 and lower C2; Figs. 3–5) are cylindrical-domal forms in plan view with positive cross-sectional relief ranging from 0.1 to 0.5 m (Figs. 8B, 11). Unlike those found in peritidal environments (e.g., Kendall and Warren 1987), they are not polygonal and differ from anticlinal structures with linear axes interpreted by Allen and Hoffman (2005) as giant wave ripples, or those attributed to growth faults by Gammon et al. (2005) in the Nuccaleena Formation in the Parachilna Gorge area of south Australia. The tepees are present as isolated structures (Fig. 11A, B) or as linked structures traceable for tens of meters in available outcrop (e.g., Fig. 11C). The cores of tepees are commonly fractured (Fig. 11A, B) and brecciated (Fig. 11C–F), and show stromatactis-like cavities (Figs. 8B, 11E). The flanks of tepees are composed of laminated dolomite with or without sheet cracks and cemented breccias. Tepees are common where the basal cap carbonate (unit C1) is disrupted and cemented (Figs. 3–5). In some cases, brecciation of tepees is intense, leading to localized collapse with overlying layers draping downwards (Fig. 11F), but their lateral linkage

indicates a genetic relationship. Overlying layers also onlap the tepees (e.g., Fig. 8B), and their exclusive occurrence within a discrete stratigraphic level at the basal cap carbonate indicates that they developed early during deposition (cf. Kennedy 1996; James et al. 2001).

Sheet Cracks.—Sheet cracks lined with dolomite, calcite, and quartz divide dolomicrite matrix into centimeter-scale units. They are found commonly on the flanks of tepee-like structures (Fig. 11A–C, E), pinch out towards the cores of those structures, and pass laterally into cemented breccias. They are also present as laterally persistent layers not directly associated with tepees, at least as far as can be determined in available outcrop. Sheet cracks are common in the most distal basal sections, where they form broad domes as much as 20 cm high and more than 2 m across. The thickness of individual sheet cracks varies from 0.5 to 3 cm, and is for the most part < 1 cm. In some cases, cement layers thicken locally into lenses 10–20 cm long and up to 5 cm thick.

Cemented Breccias.—Breccias are commonly associated with the tepees, stromatactis-like cavities, and sheet cracks described above (Figs. 3–5). Individual breccia clasts, from 2 to 8 cm across (e.g., Figs. 10, 11D–F), consist of dolomicrite and, less commonly in platform

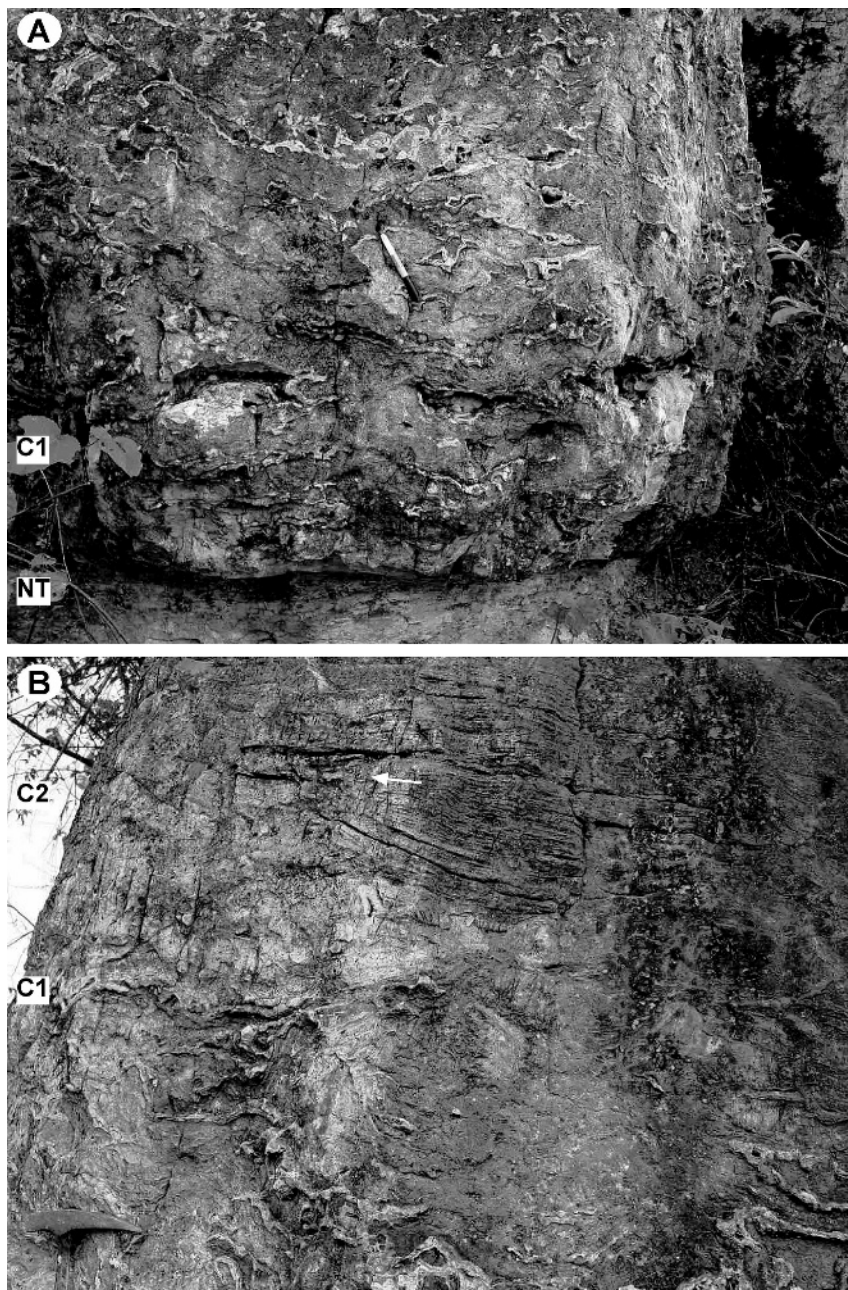


FIG. 8.—Field photos of stromatactis-like cavities of the Doushantuo cap carbonate. **A)** Stromatactis-like cavities of the basal cap carbonate (C1) directly overlie glaciogenic diamictite (NT). **B)** Linked stromatactis-like cavities extend upwards into overlying laminated dolomite (C2), forming the core of a tepee-like structure. Notice that laminated dolomite in flanks of tepees onlap towards the crest of tepees (arrow). Hammer head in the bottom left for scale. From the Liantuo section (Fig. 3B) in the Yangtze Gorge area.

sections, of micritic limestone (e.g., Figs. 3, 4A, B). Associated isopachous cements are partially replaced by quartz. In some cases, breccias and sheet cracks are approximately concordant with depositional layers. More commonly, they intersect bedding at angles of greater than 20° . The close spatial association of breccias, sheet cracks, and tepee-like structures suggests that they are genetically related.

Barite Fans.—Barite crystals line cavities (e.g., Fig. 12A). Radiating blade-shaped crystals form fans (Fig. 12B) 0.5 to 2.5 cm across, and in some cases they are partially or completely replaced by calcite and quartz. Barite rims are overgrown by early-formed isopachous cements and in turn by late-stage dolospar, consistent with early formation, probably in cavities open to marine water. Barite fans are present exclusively in association with tepee-like structures and stromatactis-like cavities, and are not found above the base of unit C2. They share a morphological

form similar to that of barite found in cold seeps described by Greinert et al. (2002a) and Torres et al. (2003).

STABLE ISOTOPES

Stable-isotope analysis of the Doushantuo cap carbonate has initially been reported in Jiang et al. (2003a) and Zhou et al. (2004). Additional measurements document the extreme isotopic heterogeneity in well-preserved limestone samples (Fig. 13) and reduced variability in dolomitized and silicified samples (Fig. 10). In the limestone crusts collected near the top of tepees, $\delta^{13}\text{C}$ values vary from -1.7‰ to -41.3‰ (Fig. 13). Larger than 30‰ variations in $\delta^{13}\text{C}$ occur within millimeters (Fig. 13). The most negative $\delta^{13}\text{C}$ values ($< -30\text{‰}$) are obtained from yellowish microcrystalline calcite and dark-gray micrite. These samples also produced higher $\delta^{18}\text{O}$ ($> -8\text{‰}$). Such isotopic heterogeneity is common in cold-seep environments where multiple sources of carbonate,

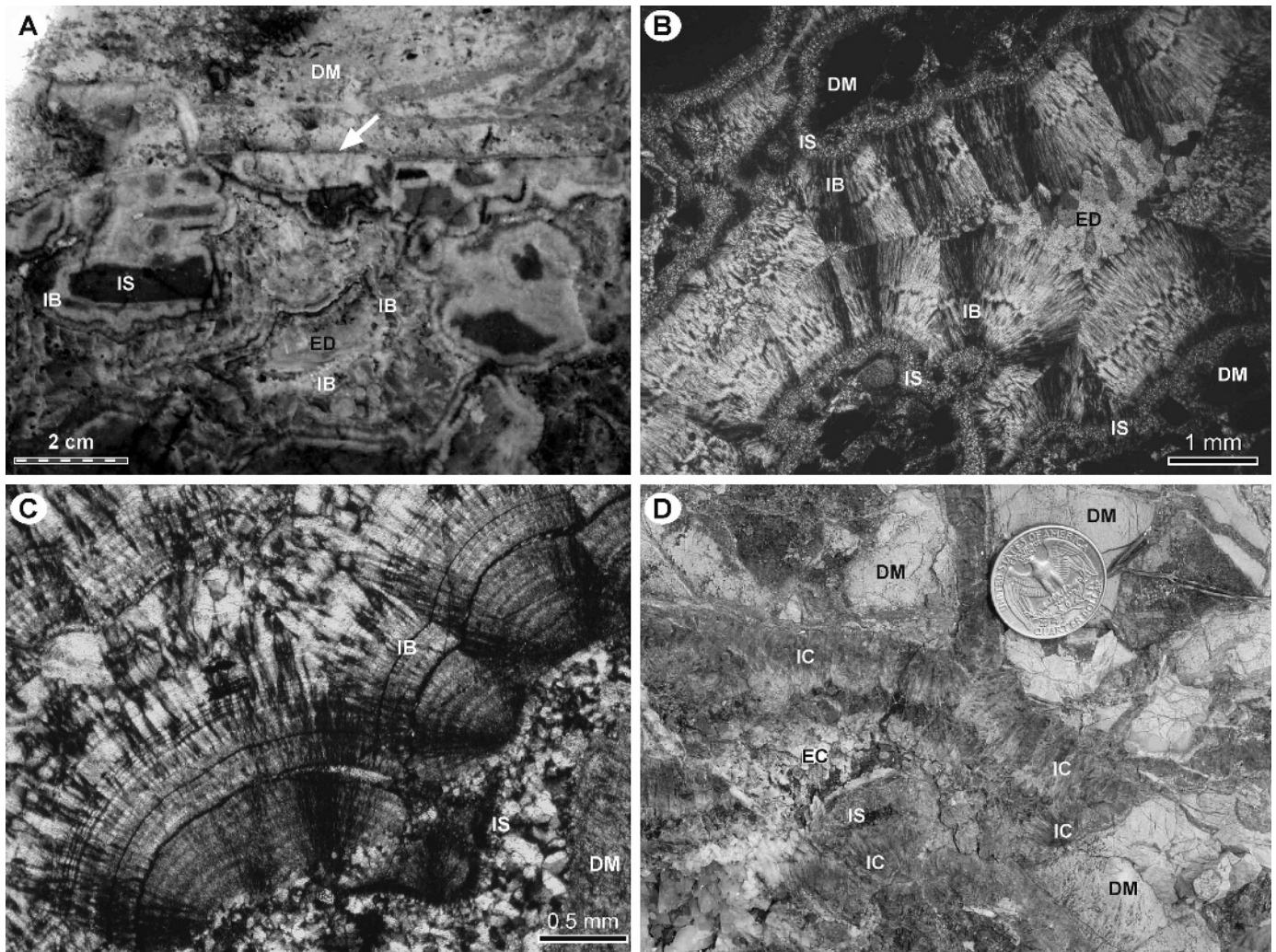


FIG. 9.—Stromatactis-like cavities and cement-filling sequences of the Doushantuo cap carbonate. **A**) Polished slab showing stromatactis-like cavities with flattened upper surface (arrow) composed of dolomicrite and cavity-filling internal sediments (IS), isopachous botryoidal cements (IB), and equant dolospar (ED). **B**) Petrography of the stromatactis-like cavity showing the growth of isopachous botryoidal cements (IB) over dolomicrite (DM) and internal sediments (IS). The remaining cavity is filled with equant dolospar (ED). Plane-polarized light. **C**) Isopachous botryoidal cements (IB) growing over dolomicrite (DM) and internal sediments (IS). Internal sediments and cements are partially replaced by silica. Plane-polarized light. **D**) Part of a stromatactis-like cavity filled by isopachous columnar fibrous calcites (IC) that grew over dolomicrite (DM) and internal sediments (IS) and equant calcite spar (EC). U.S. quarter (2.426 cm in diameter) for scale. A, B, and D are from unit C1 in Figure 3B, and C from unit C1 in Figure 4D.

stages of cementation, and metabolic pathways lead to a strongly heterogeneous isotopic composition (e.g., Peckmann et al. 2002; Campbell et al. 2002). In contrast, cavity-filling, equant calcite spar (e.g., points 1, 3, 9, 14, and 17 in Fig. 13) has less depleted $\delta^{13}\text{C}$ values ($> -8\text{‰}$) but more negative $\delta^{18}\text{O}$ values ($< -11\text{‰}$). In pervasively dolomitized and silicified sections, absolute $\delta^{13}\text{C}$ values in the basal cap carbonate (C1 and lower C2) display a much narrower range from -8‰ to -1.5‰ , and some samples from sections 13 and 14 (Fig. 5C, D) yield positive $\delta^{13}\text{C}$ values up to $+1.5\text{‰}$. Differences in $\delta^{13}\text{C}$ as large as 5‰ still exist within decimeter-size regions (e.g., Fig. 10). Oxygen isotope values are commonly $> -10\text{‰}$, except in the case of coarse late-stage calcite and dolomite spars (e.g., points 19 and 20 in Fig. 10). Such isotopic heterogeneity implies that, at least in the basal cap carbonate, both $\delta^{13}\text{C}$ and $\delta^{18}\text{O}$ values are dominated by local, pore-scale processes rather than by broader, more uniform oceanographic changes. The extreme isotopic variability in limestone samples (Fig. 13) and less variability in dolomitized samples with similar cement fabrics suggest that pervasive

dolomitization and silicification may have significantly homogenized the isotopic compositions.

DISCUSSION

Depositional Environments

Cap carbonate units are commonly interpreted as having accumulated in relatively deep water, in most cases below storm wave base (e.g., Kennedy 1996; James et al. 2001; Nogueira et al. 2003; Allen and Hoffman 2005). The Doushantuo cap carbonate shares sedimentary features with these examples: (1) the predominance of mechanically laminated micrite and dolomicrite facies and (2) the absence of such characteristically peritidal sedimentary features as ooids, microbial laminae with fenestral fabrics, desiccation cracks, and cross-stratification, or evidence for appreciable wave or tidal activity, channels, shoaling cycles, or significant lateral facies changes. However, tube structures and stromatolites, which have been documented from cap carbonates in

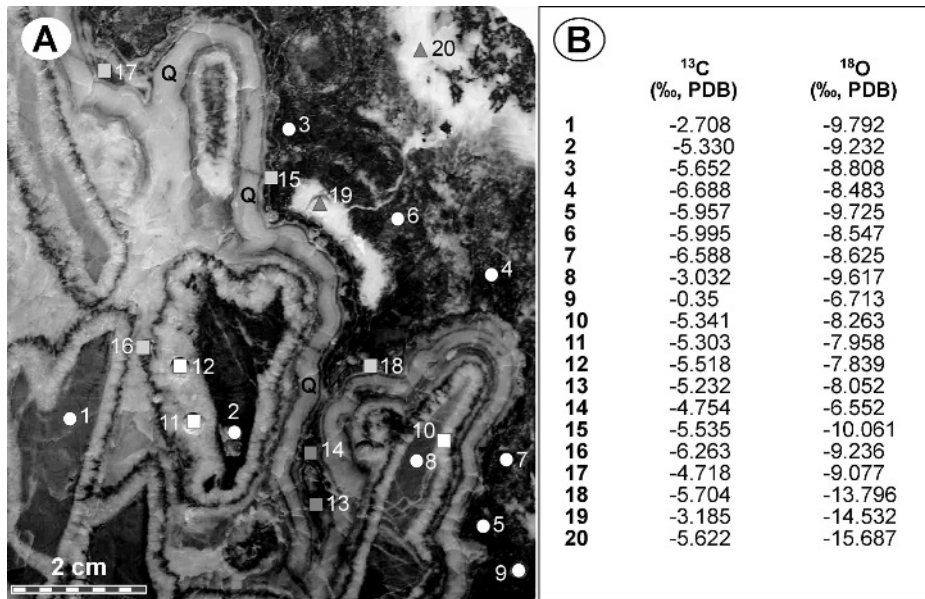


FIG. 10.—An example of cemented breccias. **A**) Hand specimen of cemented breccias from unit C1 in Figure 4D. The rock is dolomitized and partially replaced by quartz (Q). Points 1–9, dolomitic matrix; 10–18, isopachous cements; 19–20, late-stage calcite spars. **B**) Isotopic compositions of matrix and cements corresponding to points in part A. Notice up to 5‰ variations in $\delta^{13}\text{C}$ and distinctively more negative $\delta^{18}\text{O}$ values from the last-stage calcite spars (points 19 and 20).

Australia (Kennedy 1996), Namibia (Hegenberger 1987; Saylor et al. 1995; Kennedy et al. 2001; Hoffman and Schrag 2002), eastern California (Cloud et al. 1974; Kennedy et al. 2001), and Brazil (Nogueira et al. 2003), are not present in the Doushantuo cap carbonate. There is also no evidence for ice rafting in the Doushantuo, although carbonate deposition may have taken place while glacial ice was still present elsewhere on the planet, including landward of the shoreline.

The Doushantuo cap carbonate most likely accumulated in an open marine setting. Its broad distribution and the absence of evidence for a coeval stromatolitic carbonate factory argue against a shallow-marine source for the carbonate. Thin lamination suggests deposition from suspension. Normal grading and small-scale cross-lamination in some layers (Figs. 3–5) are attributed to redeposition by turbidity currents. Texturally well-preserved examples of peloids and clotted fabrics suggest precipitation of carbonate by microbially mediated processes within the water column (Chafetz 1986). Upsection trends within the cap carbonate are consistent with a decrease in carbonate saturation as available alkalinity was consumed and/or with an increase in the supply of terrigenous mud.

Interpretation of Sedimentary Structures and Textures

The close association of tepee-like structures, stromatolitic-like cavities, sheet cracks, and cemented breccias in the Doushantuo cap carbonate (Figs. 3–5) indicates that these structures are genetically related. Tepee-like structures occur exclusively at locations where stromatolitic-like cavities and sheet cracks are sufficiently well developed to cause brecciation (e.g., Figs. 8B, 11). Stratigraphically they appear in some sections at multiple horizons intercalated with stromatolitic-like cavity-bearing micritic laminae (e.g., Figs. 3A, 4A, D, 5A). Stromatolitic-like cavities, and in some cases, sheet cracks, are filled with interlayered internal sediments and isopachous cements (Fig. 9) indicative of syndepositional formation. All of these structures are restricted to a thin (< 2.5 m) basal level (C1 and lower C2; Figs. 3–5), display similar paragenetic cement sequences regardless of paleogeographic location, and are crosscut by later tectonic fractures and quartz veins, confirming their penecontemporaneous formation by the same process.

The creation of cavities (later filled by cements) and brecciated matrix within the cores of tepee-like structures, in combination with their seafloor expression, requires a force capable of buckling and splitting

partially lithified (plastic) sedimentary bedding at a very shallow depth. The roughly circular plan (domal) of these structures argues against a tectonic, growth fault, or giant wave ripple origin that would produce a linear axial trace (cf. Allen and Hoffman 2005; Gammon et al. 2005), although we do not preclude such origins for “tepee-like” or antiformal structures elsewhere. At Mt Chambers Gorge in South Australia, both types of structure are present, with the Doushantuo-like domal forms concentrated at a discrete stratigraphic level (e.g., fig. 5 in Kennedy 1996) beneath elongate forms. In the Doushantuo examples, the existence in tepee cores of stromatolitic-like cavities with varied cement morphology and mineralogy, abundant pyrite, syndepositional barite fans, internal sediments, and strongly depleted carbon isotope values (as low as -41‰ PDB) associated with specific cement generations suggest a complex early diagenetic history involving fluids of varying composition at the sea floor. These structures are not easily explained by deformation related to expansive crystallization alone (James et al. 2001), especially inasmuch as the stabilization to dolomite involves a 9% reduction in crystal volume (Arvidson and Mackenzie 1999). The lack of deformation and brecciation involving the underlying diamictite and overlying laminated carbonates, and the subvertical (to the paleohorizontal) orientation of tepees across the entire basin, do not favor seismicity-related deformation (e.g., Nogueira et al. 2003), nor does the complex diagenetic history. Rather, the creation of linked cavities and sheet cracks suggests progressive injection of gas or fluid into cohesive sediment of low permeability with buoyancy-driven buckling and failure leading to brecciation (cf. Cloud 1974), a process common in modern methane seeps (e.g., Bohrmann et al. 1998; Suess et al. 1999; Tryon et al. 2002; Van Dover et al. 2003).

In cold seeps documented from modern seafloor settings, gas ebullition from ascending methane at shallow depths dislocates pore space, creating cavities varying in size from 1 mm to 2 cm (e.g., Bohrmann et al. 1998; Suess et al. 1999; Greinert et al. 2002b). These cavities are partially filled with framboidal or acicular aragonite or high-Mg calcite cements due to localized HCO_3^- supersaturation related to anaerobic methane oxidation (e.g., Bohrmann et al. 1998; Suess et al. 1999; Greinert et al. 2002b). Vertical movement of gas and fluids is commonly impeded by hydrostatic pressure or by impermeable fine-grained sedimentary layers or newly precipitated carbonate crusts, leading to lateral injections of gas and fluid along sedimentary bedding planes and the formation of layer-parallel conduits by buoyancy-driven forces (e.g., Tryon et al. 2002; Torres et al. 2004). This is recorded by the intercalation of gas hydrate layers a few

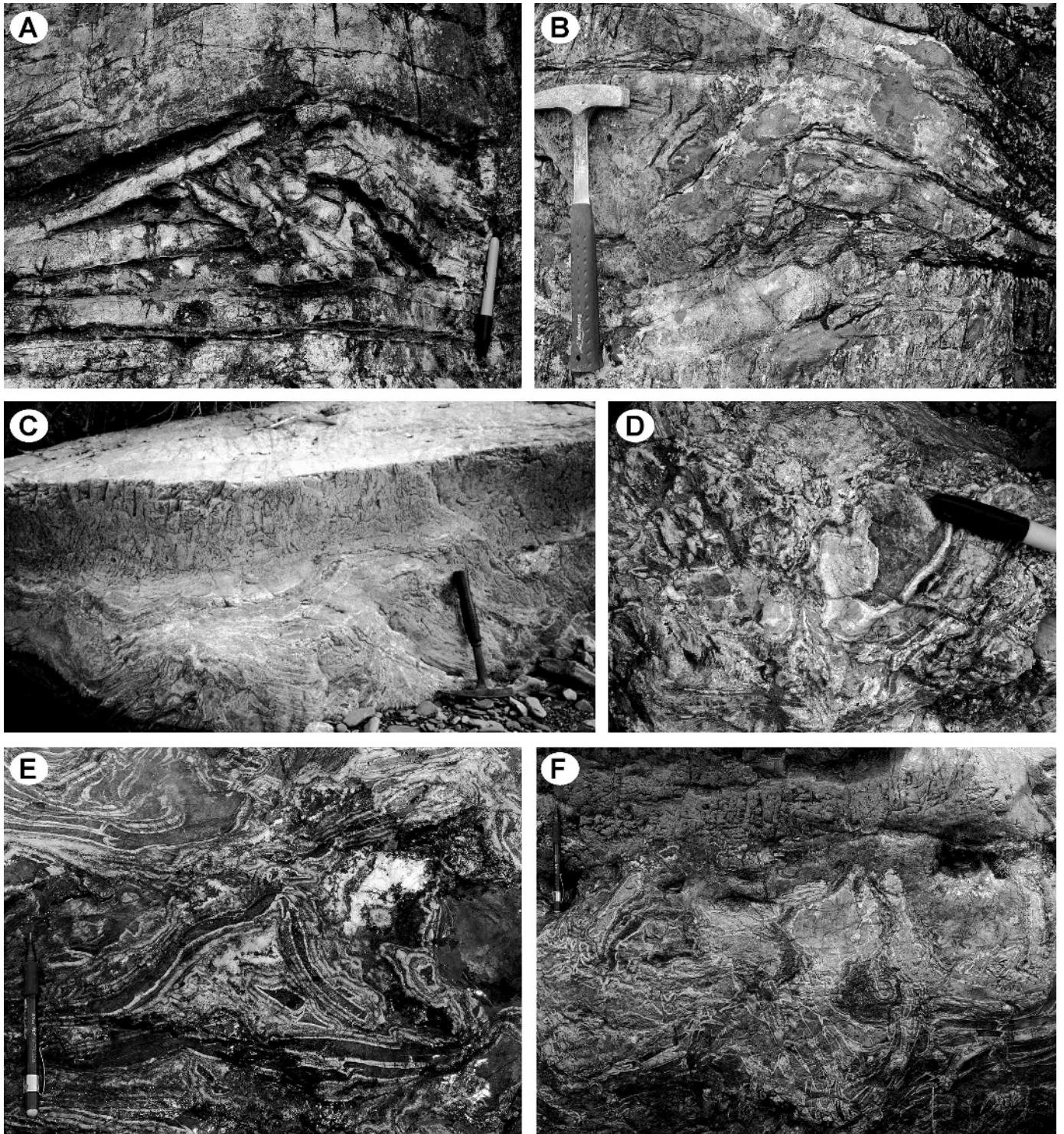


FIG. 11.—Field photos of the tepee-like structures from the Doushantuo cap carbonate. **A)** Tepee-like structure with brecciated core and layer-parallel sheet cracks in the flanks. From unit C1 in Figure 4A. **B)** A tepee-like structure expressed as an asymmetric anticline with fractured core. From unit C2 in Figure 4A. **C)** Laterally linked small tepees with brecciated and cemented cores and layer-parallel sheet cracks in flanks. From unit C1 in Figure 4D. **D)** Plan view of the core of a tepee-like structure showing breccias and isopachous cements. From unit C1 in Figure 4D. **E)** A strongly brecciated tepee-like structure with intensive isopachous cements. Stromatolite-like cavities occur in the core of the tepee. From unit C1 in Figure 4D. **F)** Collapsed tepee-like structures with downward drapes from the overlying layers. From unit C1 in Figure 4D.

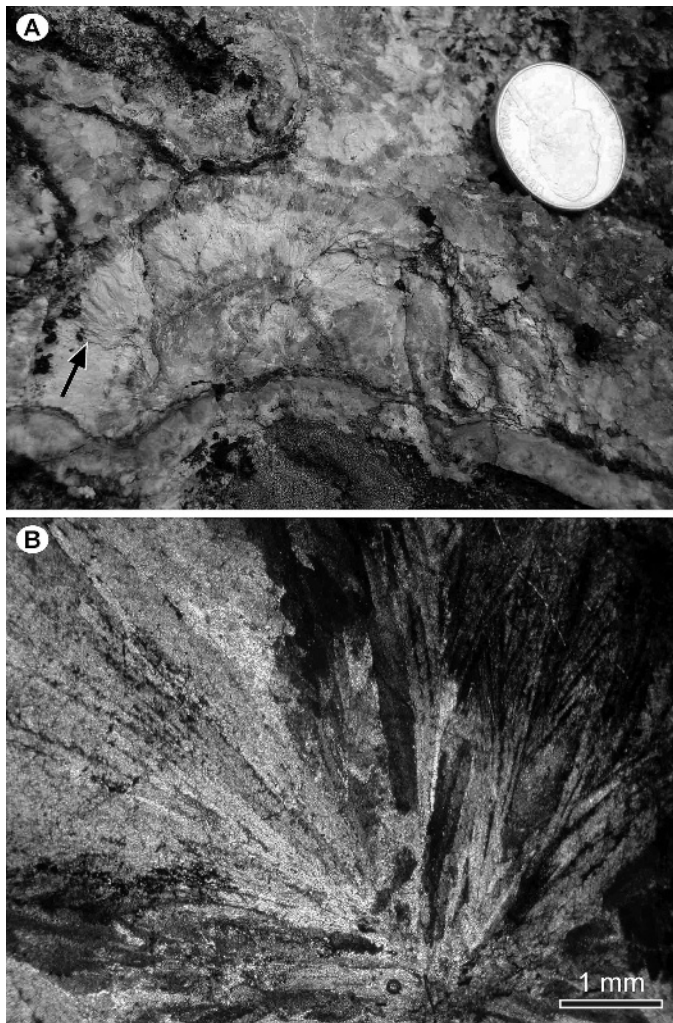


FIG. 12.—Barite from Doushantuo cap carbonate. **A**) Barite fans filling a stromatactis-like cavity. Barite fan is overlain by isopachous cements suggesting early formation. U.S. nickel (2.121 cm in diameter) for scale. **B**) Thin-section photograph showing radiating blade-shaped barite crystals. Barite is now partially replaced by calcite. Plane-polarized light. From unit C1 in Figure 4G.

millimeters to 10 cm thick within muddy sediment surrounding cold seeps (e.g., Hydrate Ridge off Oregon; Bohrmann et al. 1998; Suess et al. 1999; Suess et al. 2001). At locations characterized by gas buildup, elevated pressure may result in the lateral movement of gas or fluid, with vigorous gas release ultimately driving intense fracturing and brecciation (Hovland et al. 1987; Bohrmann et al. 1998; Suess et al. 2001; Torres et al. 2002; Tryon et al. 2002; MacDonald et al. 2003). Modern and ancient seeps are thus characterized by distinctive cement-lined, interconnected cavities and sheet cracks formed by gas buoyancy with a common flat topped stromatactis-like form. The seafloor position of these seeps provides both the seawater and seep-derived reactants required for metabolism by a complex microbial community, and it accounts for the several phases of carbonate cement, dissolution, accumulation of both reduced (pyrite) and oxidized sulfur (barite), and extremely variable carbon isotope values at a millimetric scale (Kulm and Suess 1990; Kelly et al. 1995; Kauffman et al. 1996; Bohrmann et al. 1998; Cavagna et al. 1999; Stakes et al. 1999; Peckmann et al. 2002; Campbell et al. 2002; Suess et al. 1999; Suess et al. 2001; Tryon et al. 2002; Peckmann and Thiel 2004).

The distinctive suite of sedimentary structures and textures in the Doushantuo cap carbonate is remarkably similar to features observed in modern methane seeps and other inferred ancient analogues. Linked sheet cracks and stromatactis-like cavities in the basal Doushantuo cap carbonate (unit C1) vary in sizes from < 0.5 cm to 5 cm and are lined with pyrite-rich isopachous botryoidal or columnar cements (Fig. 9), consistent with the creation of cavities by lateral (along bedding planes) and vertical (between cavities) gas expulsion in cohesive pelagic or hemipelagic carbonate mud of low permeability. Flat-roofed stromatactis-like cavities (e.g., Fig. 9A) suggests downward-directed precipitation due to gas buoyancy, similar to examples documented from modern (e.g., Greinert et al. 2002b) and ancient (e.g., Peckmann et al. 2002; Peckmann and Thiel 2004) methane seeps. Fracturing, brecciation, and the development of cavities within the tepee-like structures (Figs. 8B, 11) are consistent with locally elevated pressure and vigorous gas venting. Pyrite and barite, combined with strongly depleted carbon isotope values (-41% PDB), suggest an origin from sulfate oxidation of methane by a microbial consortium.

Bedding-parallel dissolution features in the upper cap carbonate (unit C3; Figs. 4E, G, 5C) may reflect a change in lysocline depth related to methane oxidation (e.g., Dickens et al. 1997) or changes in local chemical composition such as higher HS^- concentration common around seeps (e.g., Campbell et al. 2002). More work is needed to elucidate such details, particularly sulfur isotope studies of pyrite.

Carbon isotope values as low as -41% in well-preserved limestone crusts within the tepees (Fig. 13; Jiang et al. 2003a) provide unequivocal evidence for methane influence that, when considered in context with the other seep-related features, argues strongly against a diagenetic methane production from *in situ* marine organic matter (methanogenesis) for these isotopic values (e.g., Shields 2005). Detailed isotopic mapping of hand samples within the interpreted seep facies (Fig. 13) illustrates the limited spatial distribution of carbonate demonstrably related to a methane source of carbon. Typical sampling practices would not identify methane as a contributor, because the bulk $\delta^{13}\text{C}$ composition of this sample is -6% . Though variability at this scale is typical of seeps (Peckmann et al. 2002; Campbell et al. 2002), homogenization of isotopic values is enhanced within the Doushantuo cap carbonate by dolomitization (Jiang et al. 2003a). Other sections in the Doushantuo cap carbonate with a similar suite of sedimentary structures lack diagnostic carbon isotope values for methane influence, showing almost no variability beyond the bulk-rock isotopic value of the basal cap carbonate (unit C1; $\delta^{13}\text{C} \approx -5\%$), an influence that is not uncommon in other ancient seep examples (e.g., Aiello et al. 2001; Campbell et al. 2002). The Doushantuo cap carbonate is also the only example documented that locally retains a primary limestone mineralogy (excluding laminated limestone above the cap level in the Maieberg Formation of Namibia and the Hayhook Formation in the Mackenzie Mountains of northwestern Canada; Hoffman et al. 1998; James et al. 2001; Porter et al. 2004). It thus serves as an important geochemical window into the diverse primary processes that affected carbonate precipitation at seep-like structures and their diagenetic homogenization during dolomitization, and by extension to other interpreted seep-like structures in other dolomitized cap carbonates globally (e.g., Kennedy et al. 2001). The widespread distribution of similar distinctive sedimentary structures and textures suggests a broader role for methane release at the end of the Marinoan ice age.

Distribution and Timing of Methane Release

Modern gas hydrates are stabilized beneath the seafloor ($\sim 99\%$) and polar permafrost ($< 1\%$) because of the delicate balance of temperature ($< 7^\circ\text{C}$) and hydrostatic pressure (> 50 bar; Haq 1998; Kvenvolden 1998). The hydrate stability zone lies below 300 m water depth at continental margins and as shallow as 100 m below polar permafrost

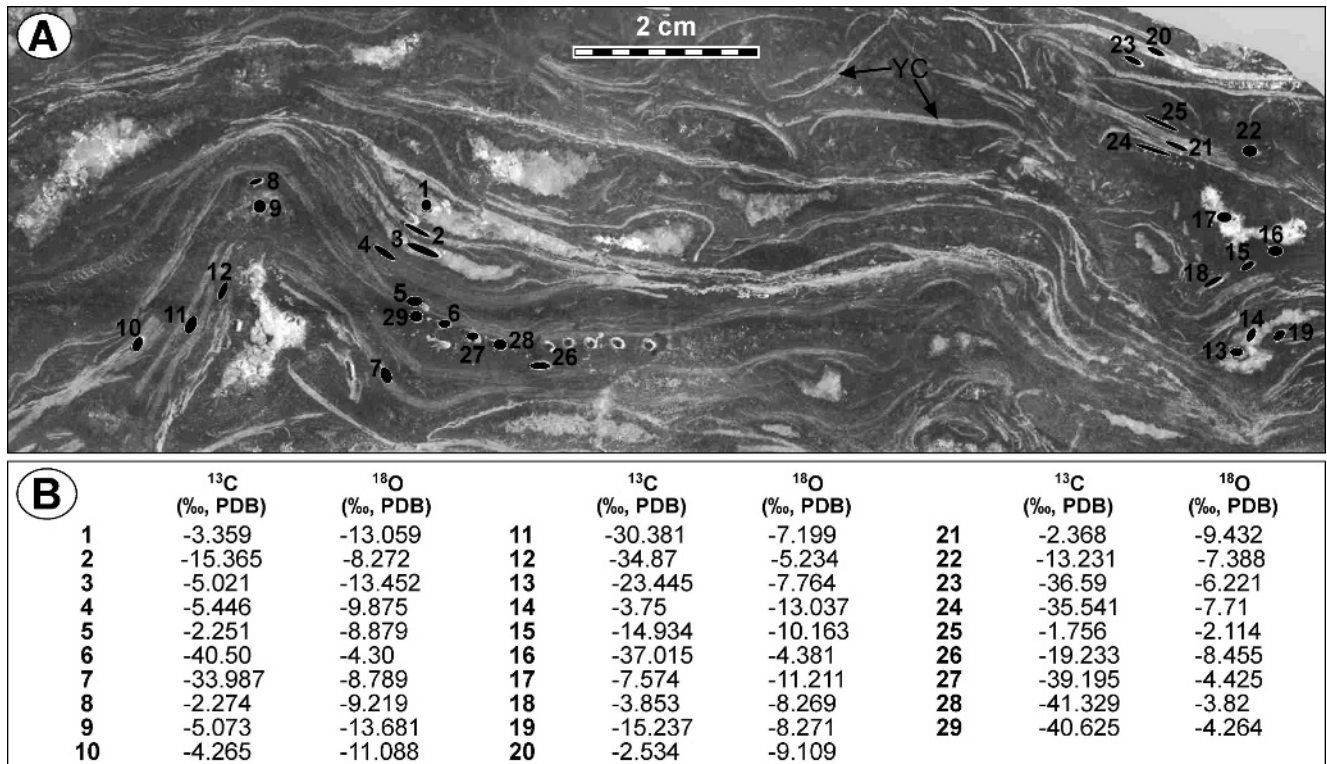


Fig. 13.—Isotopic compositions from a limestone crust right above a tepee-like structure in Figure 4A (2.1 m in the column). Notice the large $\delta^{13}\text{C}$ variations (up to 30‰) at millimeter to centimeter scales. The most negative $\delta^{13}\text{C}$ values ($< -30\%$) with relatively heavy $\delta^{18}\text{O}$ values ($> -8\%$) are from yellowish microcrystalline limestone (YC) and dark-gray micrite (points 6, 7, 11, 12, 23, 24, 27, 28, 29), while cavity-filling calcite spars (e.g., points 1, 3, 9, 14, and 17) have less depleted $\delta^{13}\text{C}$ ($> -8\%$) but more negative $\delta^{18}\text{O}$ values ($< -11\%$).

(Kvenvolden 1998; Buffett 2000). During times of extremely cold climate such as the Marinoan, the hydrate stability zone would have been appreciably shallower because of low temperatures or the pressure of ice. Subsequent warming during deglaciation would have destabilized the gas hydrates, releasing methane widely at continental margins. If the sedimentary structures and textures in the Doushantuo cap carbonate (Figs. 2–5) are methane-related, their localized expression but widespread distribution, independent of paleogeographic setting or paleowater depth, suggests a basin-scale destabilization of gas hydrate that would likely be dominated by marine sources but could involve terrestrial permafrost as well (Kennedy et al. 2001). Postglacial warming is inferred to have been sufficiently great, even in the deep ocean, to destabilize the entire gas-hydrate inventory.

The restriction of the distinctive sedimentary structures and textures to the hemipelagic and pelagic deposits of the basal cap carbonate (C1) in each platform-to-basin transect (Figs. 3–5) provides an important constraint on the timing of methane release. The basal cap carbonate (C1) is strongly disrupted, with abundant stromatolite-like cavities appearing at the lower contact and extending upward into the base of unit C2. We infer that methane release began during the deposition of unit C1, and perhaps earlier. Direct physical evidence would be recognized with difficulty in diamictite given the significant difference in permeability. Methane release ceased during the deposition of unit C2.

Methane Release in a Supersaturated Ocean: an Explanation for Cap Carbonates and Their Associated $\delta^{13}\text{C}$ Anomaly

The stratigraphy, sedimentary structures, and textures of the Doushantuo cap carbonate, in combination with the $\delta^{13}\text{C}$ anomaly and similar physical features from other cap carbonate examples (e.g., Kennedy et al.

2001), support the widespread release of methane at the end of the Marinoan glaciation (Fig. 14). Methane released by gas-hydrate destabilization could have been oxidized either anaerobically (e.g., Boetius et al. 2000) or aerobically (e.g., Katz et al. 1999).

Anaerobic methane oxidation ($\text{CH}_4 + \text{SO}_4^{2-} \rightarrow \text{HCO}_3^- + \text{HS}^- + \text{H}_2\text{O}$; Fig. 14A) has two important consequences. One is the localized supersaturation of HCO_3^- near the seawater–sediment contact and in pore fluids, leading to precipitation of carbonate crusts and cements. Such crusts and cements would have a wide range of $\delta^{13}\text{C}$ values, from -50% to $+6\%$ (e.g., Kaufmann et al. 1996; Aiello et al. 2001; Campbell et al. 2002; Peckmann et al. 2002; Formolo et al. 2004; Peckmann and Thiel 2004), depending on the hydrocarbon source, ambient seawater mixing ratio, and subsequent diagenetic stabilization. This expectation is consistent with our data for carbonate cements in the Doushantuo cap carbonate. As is the case for many modern and ancient examples of methane seeps, only rarely is the full range of carbon isotope values preserved, owing to isotopic homogenization during diagenesis (Aiello et al. 2001; Campbell et al. 2002; Jiang et al. 2003a). A second consequence of anaerobic methane oxidation is a corresponding positive seawater sulfur isotope excursion and a substantial reduction in the standing stock of sulfate in seawater from the anaerobic oxidation of methane by sulfate. This is consistent with the nadir in seawater sulfate concentration and the positive $\delta^{34}\text{S}$ values at the upper cap carbonate level reported in the literature (e.g., Hurtgen et al. 2002; Zhang et al. 2003).

A portion of the methane released into the ocean would have been oxidized aerobically to CO_2 ($\text{CH}_4 + 2\text{O}_2 \rightarrow \text{CO}_2 + 2\text{H}_2\text{O}$; Fig. 14A, B), either in the water column or in the atmosphere. A pulse of methane-derived CO_2 would have led to carbonate dissolution and conceivably to a rise in the lysocline (e.g., Dickens et al. 1997). Over longer timescales, however, this ^{12}C -enriched source of carbon would lead to the precipitation of carbonate, possibly driving the negative $\delta^{13}\text{C}$ excursion

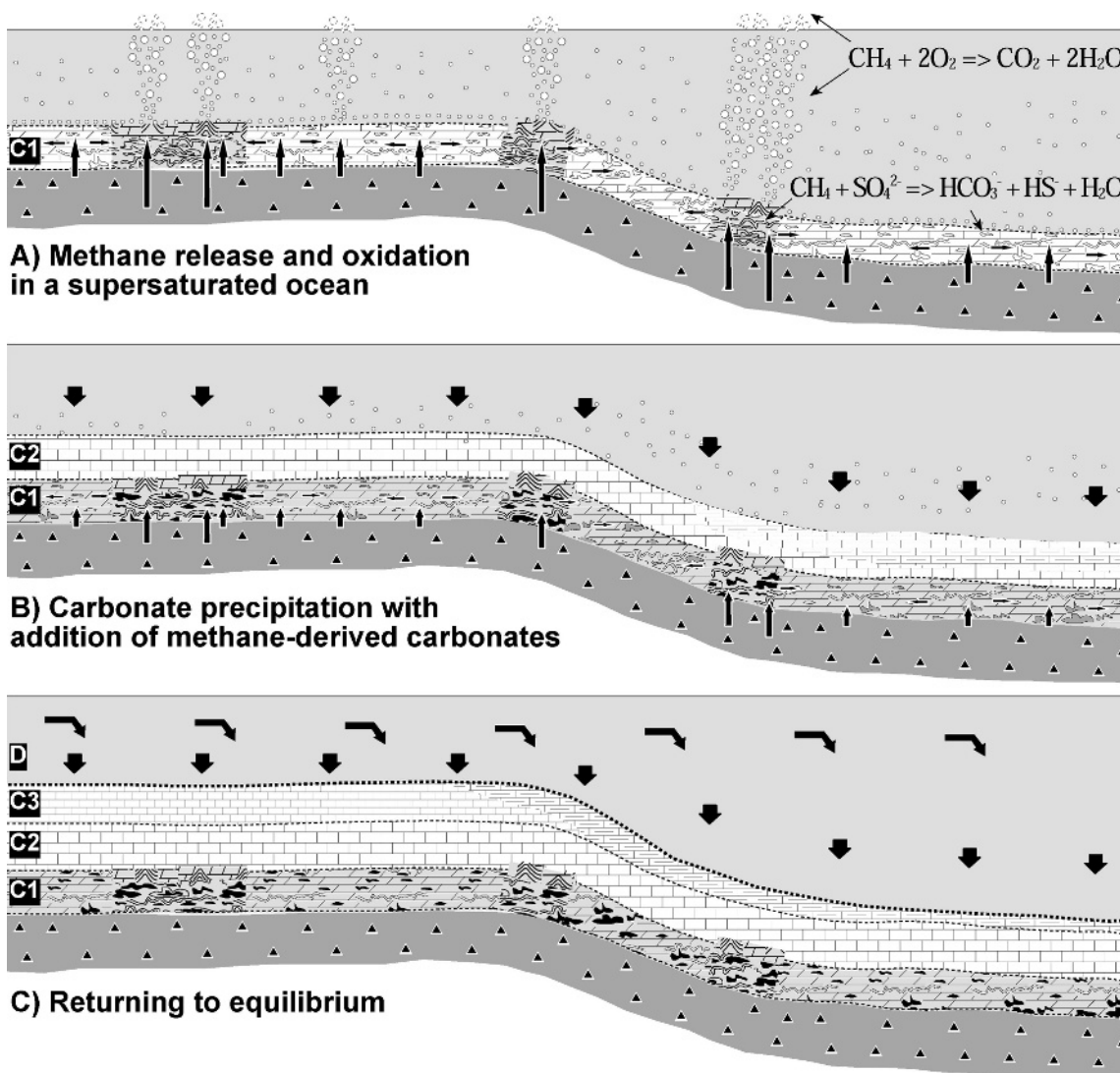


FIG. 14.—Hypothetical model for methane release in a supersaturated ocean based on the Doushantuo cap carbonate stratigraphy, sedimentary structures, and isotopic trends. **A)** Methane release from destabilization of gas hydrate into the supersaturated ocean during C1 deposition. Methane gas and fluids physically disrupt bedding, resulting in formation of observed structures. Methane may have been partially oxidized anaerobically ($\text{CH}_4 + \text{SO}_4^{2-} \rightarrow \text{HCO}_3^- + \text{HS}^- + \text{H}_2\text{O}$) near seawater–sediment contact, leading to precipitation of carbonate crusts and cements. Assuming that seawater was supersaturated, precipitation of crusts and cements would have involved carbonate ions already in the seawater, resulting in the mixing of isotopically different carbon sources in carbonate crusts and cements. Methane could also have been partially oxidized aerobically ($\text{CH}_4 + 2\text{O}_2 \rightarrow \text{CO}_2 + 2\text{H}_2\text{O}$) in the water column and/or in the atmosphere to produce CO_2 , causing ocean anoxia and potential fluctuation of atmospheric oxygen concentration. **B)** Methane release ended by the time of deposition of the upper part of unit C2, and methane-derived carbon joined the existing alkalinity in the ocean to precipitate units C2 and C3, resulting in basinal to global $\delta^{13}\text{C}$ excursion. **C)** Carbonate precipitation and/or increase of terrigenous mud finally consumed and/or diluted the supersaturation state of seawater, which returned gradually to normal condition.

recorded by the Doushantuo and other cap carbonates. More importantly, aerobic methane oxidation in the water column may have resulted in oxygen drawdown, causing a marine biotic crisis (e.g., Harries and Little 1999; Hesselbo et al. 2000) and fluctuation in atmospheric oxygen. If the negative $\delta^{13}\text{C}$ excursion (estimated as -4‰ to -7‰ ; Jiang et al. 2003a) recorded by cap carbonates represents a global event caused by the addition of methane to the seawater and atmosphere, it would need ~ 2.5 to $\sim 4.3 \times 10^{17}$ moles of CH_4 (Kennedy et al. 2001; Jiang et al. 2003a). Aerobic oxidization ($\text{CH}_4 + 2\text{O}_2 \rightarrow \text{CO}_2 + 2\text{H}_2\text{O}$) of this amount of methane would require ~ 5.0 to $\sim 8.6 \times 10^{17}$ moles of O_2 , which is more than twice to four times the total amount of free oxygen stored in modern seawater ($\sim 2.0 \times 10^{17}$ moles of O_2). We recognize the

uncertainties inherent in such estimates, related in part to uncertainties in the partial pressure of oxygen in the Neoproterozoic atmosphere and the sulfate concentration of seawater. It is nevertheless conceivable that methane hydrate destabilization could have driven the oceans towards anoxia, influencing biological innovation during this critical period of time. Strong variations in the partial pressure of oxygen mediated by the methane cycle may have played an influential role in metazoan evolution (e.g., Knoll and Holland 1995; Runnegar 2000).

Methane release in a supersaturated ocean (Fig. 14) provides a simple yet compelling explanation for the sedimentary structures, textures, and associated carbon isotope excursion of cap carbonates. The sources of carbonate alkalinity responsible for the supersaturation of the ocean

during the precipitation of the carbonate are not as well established. Mass-balance considerations (cf. Dickens et al. 1995) indicate that even if the entire present-day gas-hydrate reservoir were destabilized (e.g., Kvenvolden 1988, 2002; Haq 1999), only about 1.0×10^{19} g of carbon would be made available. That is roughly equivalent to 1.2 m of carbonate distributed over an area comparable to the present-day continental shelves. However, considering the extremely cold climate during Marinoan ice age, a much larger methane-hydrate inventory was possible. Additional sources of alkalinity contributing to cap-carbonate deposition may include (1) continental weathering during deglaciation (Hoffman et al. 1998; Higgins and Schrag 2003), (2) alkalinity retained in seawater as a result of stratification (Grotzinger and Knoll 1995; Knoll et al. 1996; Kaufman et al. 1997), and (3) excess alkalinity sequestered within the glacial ocean and redelivered to the shelf during transgression (Ridgwell et al. 2003; Ridgwell and Kennedy 2004).

CONCLUSIONS

The Doushantuo cap carbonate (ca. 635 Ma), less than 5 m thick, overlying the glaciogenic Nantuo Formation in south China is interpreted as having accumulated in relatively deep water (below storm wave base) during deglaciation. Localized stromatolite-like cavities, tepee-like structures, sheet cracks, and associated breccias, along with barite fans, abundant pyrite, and multiple generations of carbonate cement with strongly depleted carbon isotope values in the basal units of this carbonate are interpreted as ancient methane seeps formed by comparatively short-lived gas-hydrate destabilization in the aftermath of a severe glaciation. The presence of methane-related sedimentary structures and textures even in the deep basin suggests that postglacial warming was sufficient to destabilize the marine gas-hydrate inventory as well as any permafrost-related hydrates. The Doushantuo Formation provides one of the best preserved examples of a cap carbonate, at least locally retaining primary mineralogy and isotopic variability. It thus provides a rare opportunity to examine the primary processes that may have resulted in the enigmatic sedimentary structures and textures endemic to other Marinoan age cap carbonates globally.

Widespread postglacial methane release provides a simple yet compelling explanation for the sedimentary structures, textures, and associated carbon isotope excursion of the Doushantuo cap carbonate and other cap carbonates globally. This event may have important implications for the oxygen budget and hence for biological innovation during the latest Neoproterozoic (the Ediacaran Period). Refining the timing and trigger of gas-hydrate destabilization, quantifying methane oxidation in the water column and resultant ocean anoxia, and elucidating biological details through cap carbonates into overlying strata offer a test of this hypothesis.

ACKNOWLEDGMENTS

We thank Ziqiang Wang, Xiaoying Shi, Linzhi Gao, Chongyu Yin, Yongqing Liu, Yangeng Wang, Niting Wang, Yongqi Chen, Xiaohong Chen, and Xiaofeng Wang for their guidance and discussions on the best outcrops and representative sections; and Dameng Liu, Guobiao Li, and their students for assistance in preparing and shipping the samples. David D. Mrofka and Thomas Bristow at the University of California, Riverside, conducted the isotopic analysis and contributed to the discussions in the field. Discussions with Professor Yongfei Zheng helped to improve the sections related to the tectonic history of south China. We express our sincere appreciation to Drs. Katherine A. Giles (Associate Editor), Daniel J. Lehrmann, an anonymous reviewer, and Journal Editor Kitty Milliken, who reviewed the manuscript and provided many valuable suggestions that significantly improved the paper. Editorial work by Dr. John B. Southard is also highly appreciated. This research is supported by National Science Foundation grants EAR0345207 and EAR0345642.

REFERENCES

- AIELLO, I.W., GARRISON, R.E., MOORE, J.C., KASTNER, M., AND STAKES, D.S., 2001, Anatomy and origin of carbonate structures in a Miocene cold-seep field: *Geology*, v. 29, p. 1111–1114.
- AITKEN, J.D., 1991, Two late Proterozoic glaciations, Mackenzie Mountains, northwestern Canada: *Geology*, v. 19, p. 445–448.
- ALLEN, P.A., AND HOFFMAN, P.F., 2005, Extreme winds and waves in the aftermath of a Neoproterozoic glaciation: *Nature*, v. 433, p. 123–127.
- AMTHOR, J.E., GROTZINGER, J.P., SCHRODER, S., BOWRING, S.A., RAMEZANI, J., MARTIN, M.W., AND MATTER, A., 2003, Extinction of *Cloudia* and *Namacalathus* at the Precambrian–Cambrian boundary in Oman: *Geology*, v. 31, p. 431–434.
- ARVIDSON, R.S., AND MACKENZIE, F.T., 1999, The dolomite problem: control of precipitation kinetics by temperature and saturation state: *American Journal of Science*, v. 299, p. 257–288.
- BARFOD, G.H., ALBAREDE, F., KNOLL, A.H., XIAO, S., TELOUK, P., FREL, R., AND BAKER, J., 2002, New Lu–Hf and Pb–Pb age constraints on the earliest animal fossils: *Earth and Planetary Science Letters*, v. 201, p. 203–212.
- BOETIUS, A., RAVENSCHLAG, K., SCHUBERT, C.J., RICKERT, D., WIDDEL, F., GIESEKE, A., AMANN, R., JORGENSEN, B.B., WITTE, U., AND PFANNKUCHE, O., 2000, A marine microbial consortium apparently mediating anaerobic oxidation of methane: *Nature*, v. 407, p. 623–626.
- BOHRMANN, G., GREINERT, J., SUESS, E., AND TORRES, M., 1998, Authigenic carbonates from the Cascadia subduction zone and their relation to gas hydrate stability: *Geology*, v. 26, p. 647–650.
- BOURQUE, P.-A., AND BOULVAIN, F., 1993, A model for the origin and petrogenesis of the red stromatolite limestone of Paleozoic carbonate mounds: *Journal of Sedimentary Petrology*, v. 63, p. 607–619.
- BOWRING, S.A., AND ERWIN, D.H., 1998, A new look at evolutionary rates in deep time: uniting paleontology and high-precision geochronology: *GSA Today*, v. 89, p. 1–8.
- BUFFETT, B.A., 2000, Clathrate hydrates: *Annual Review of Earth and Planetary Sciences*, v. 28, p. 477–507.
- CAMPBELL, K.A., FARMER, J.D., AND DES MARAIS, D., 2002, Ancient hydrocarbon seeps from the Mesozoic convergent margin of California: carbonate geochemistry, fluids and palaeoenvironments: *Geofluids*, v. 2, p. 63–94.
- CAVAGNA, S., CLARI, P., MARTIRE, L., AND CAMOIN, G.F., 1999, The role of bacteria in the formation of cold seep carbonates: geological evidence from Monferrato (Tertiary, NW Italy): *Sedimentary Geology*, v. 126, p. 253–270.
- CHAFETZ, H.S., 1986, Marine peloids: a product of bacterially induced precipitation of calcite: *Journal of Sedimentary Petrology*, v. 56, p. 812–817.
- CHEN, D.F., DONG, W.Q., ZHU, B.Q., AND CHEN, X.P., 2004, Pb–Pb ages of Neoproterozoic Doushantuo phosphorites in South China: constraints on early metazoan evolution and glaciation events: *Precambrian Research*, v. 132, p. 123–132.
- CLOUD, P., WRIGHT, L.A., WILLIAMS, E.G., DIEHL, P.E., AND WALTER, M.R., 1974, Giant stromatolites and associated vertical tubes from the Upper Proterozoic Noonday Dolomite, Death Valley region, eastern California: *Geological Society of America, Bulletin*, v. 85, p. 1869–1882.
- COMPSTON, W., WILLIAMS, I.S., KIRSCHVINK, J.L., ZHANG, Z., AND MA, G., 1992, Zircon U–Pb ages for the Early Cambrian time-scale: *Geological Society of London, Journal*, v. 149, Part 2, p. 171–184.
- CONDON, D., ZHU, M., BOWRING, S., WANG, W., YANG, A., AND JIN, Y., 2005, U–Pb Ages from the Neoproterozoic Doushantuo Formation, China: *Science*, v. 308, p. 95–98.
- DE ALVARENGA, C.J.S., SANTOS, R.V., AND DANTAS, E.L., 2004, C–O–Sr isotopic stratigraphy of cap carbonates overlying Marinoan-age glacial diamictites in the Paraguanay Belt, Brazil: *Precambrian Research*, v. 131, p. 1–21.
- DEYNOUX, M., TROMPETTE, R., AND SCHERMERHORN, L.J.G., 1976, Late Precambrian mixtites: glacial and/or nonglacial? Dealing especially with the mixtites of West Africa: *American Journal of Science*, v. 276, p. 1302–1315.
- DICKENS, G.R., CASTILLO, M.M., AND WALKER, J.C.G., 1997, A blast of gas in the latest Paleocene: simulating first-order effects of massive dissociation of oceanic methane hydrate: *Geology*, v. 25, p. 259–262.
- DICKENS, G.R., O'NEIL, J.R., REA, D.K., AND OWEN, R.M., 1995, Dissociation of oceanic methane hydrate as a cause of the carbon isotope excursion at the end of the Paleocene: *Paleoceanography*, v. 10, p. 965–971.
- FORMOLO, M.J., LYONS, T.W., ZHANG, C., KELLEY, C., SASSEN, R., HORITA, J., AND COLE, D.R., 2004, Quantifying carbon sources in the formation of authigenic carbonates at gas hydrate sites in the Gulf of Mexico: *Chemical Geology*, v. 205, p. 253–264.
- GAMMON, P.R., MCKIRDY, D.M., AND SMITH, H.D., 2005, The timing and environment of tepee formation in a Marinoan cap carbonate: *Sedimentary Geology*, v. 177, p. 195–208.
- GREINERT, J., BOLLWERK, S.M., DERKACHEV, A., BOHRMANN, G., AND SUESS, E., 2002a, Massive barite deposits and carbonate mineralization in the Derugin Basin, Sea of Okhotsk: precipitation processes at cold seep sites: *Earth and Planetary Science Letters*, v. 203, p. 165–180.
- GREINERT, J., BOHRMANN, G., AND ELVERT, M., 2002b, Stromatolitic fabric of authigenic carbonate crusts: results of anaerobic methane oxidation at cold seeps in 4,850 m water depth: *International Journal of Earth Sciences*, v. 91, p. 698–711.
- GROTZINGER, J.P., AND KNOLL, A.H., 1995, Anomalous carbonate precipitates: is the Precambrian the key to the Permian? *Palaios*, v. 10, p. 578–596.

- GROTZINGER, J.P., BOWRING, S.A., SAYLOR, B.Z., AND KAUFMAN, A.J., 1995, Biostratigraphic and geochronologic constraints on early animal evolution: *Science*, v. 270, p. 598–604.
- HALVERSON, G.P., MALOOF, A.C., AND HOFFMAN, P.F., 2004, The Marinoan glaciation (Neoproterozoic) in northeast Svalbard: *Basin Research*, v. 16, p. 297–324.
- HAQ, B.U., 1998, Natural gas hydrates: searching for the long-term climatic and slope-stability records, in Henriet, J.-P., and Mienert, J., eds., *Gas Hydrate: Relevance to World Margin Stability and Climate Change*: Geological Society of London, Special Publication 137, p. 303–318.
- HAQ, B.U., 1999, Methane in the deep blue sea: *Science*, v. 285, p. 543–544.
- HARRIES, P.J., AND LITTLE, C.T.S., 1999, The early Toarcian (Early Jurassic) and the Cenomanian–Turonian (Late Cretaceous) mass extinctions; similarities and contrasts: *Palaeogeography, Palaeoclimatology, Palaeoecology*, v. 154, p. 39–66.
- HEGENBERGER, W., 1987, Gas escape structures in Precambrian peritidal carbonate rocks: *Geological Survey of southwest Africa/Namibia, Communications*, v. 3, p. 49–55.
- HESELBO, S.P., GROCKE, D.R., JENKINS, H.C., BJERRUM, C.J., FARRIMOND, P., MORGANS BELL, H.S., AND GREEN, O.R., 2000, Massive dissociation of gas hydrate during a Jurassic oceanic anoxic event: *Nature*, v. 406, p. 392–395.
- HIGGINS, J.A., AND SCHRAG, D.P., 2003, Aftermath of a snowball Earth: *Geochemistry Geophysics Geosystems*, v. 4, p. 1–20 (doi: 10.1029/2002GC000403).
- HLADIL, J., 2005, The formation of stromatolite-type fenestral structures during the sedimentation of experimental slurries—a possible clue to a 120-year-old puzzle about stromatolites: *Bulletin of Geosciences (Prague)*, v. 80, p. 193–211.
- HOFFMAN, P.F., AND SCHRAG, D.P., 2002, The snowball Earth hypothesis: testing the limits of global change: *Terra Nova*, v. 14, p. 129–155.
- HOFFMAN, P.F., KAUFMAN, A.J., HALVERSON, G.P., AND SCHRAG, D.P., 1998, A Neoproterozoic snowball earth: *Science*, v. 281, p. 1342–1346.
- HOVLAND, M., TALBOUT, M., QVALE, H., OLAUSSON, S., AND AASBERG, L., 1987, Methane-related carbonate cements in pockmarks of the North Sea: *Journal of Sedimentary Petrology*, v. 57, p. 881–892.
- HURTGEN, M.T., ARTHUR, M.A., SUITS, N.S., AND KAUFMAN, A.J., 2002, The sulfur isotopic composition of Neoproterozoic seawater sulfate: implications for a snowball Earth?: *Earth and Planetary Science Letters*, v. 203, p. 413–429.
- JAMES, N.P., AND CHOQUETTE, P.W., 1990, Carbonate diagenesis on the modern and ancient sea floor, meteoric diagenesis and diagenesis in the zone of mixed waters, in Bloy, G.R., and Hadley, M.G., eds., *The Development of Porosity in Carbonate Reservoirs: Short Course Notes*: Canadian Society of Petroleum Geologists, Canada.
- JAMES, N.P., NARBONNE, G.M., AND KYSER, T.K., 2001, Late Neoproterozoic cap carbonates: Mackenzie Mountains, northwestern Canada: precipitation and global glacial meltdown: *Canadian Journal of Earth Sciences*, v. 38, p. 1229–1262.
- JIANG, G., WANG, Z., AND ZHANG, L., 1996, Sequence stratigraphy of upper Proterozoic glacial rocks in southeastern margin of Yangtze Platform: *Journal of China University of Geosciences*, v. 7, p. 38–45.
- JIANG, G., KENNEDY, M.J., AND CHRISTIE-BLICK, N., 2003a, Stable isotopic evidence for methane seeps in Neoproterozoic postglacial cap carbonates: *Nature*, v. 426, p. 822–826.
- JIANG, G., SOHL, L.E., AND CHRISTIE-BLICK, N., 2003b, Neoproterozoic stratigraphic comparison of the Lesser Himalaya (India) and Yangtze Block (South China): paleogeographic implications: *Geology*, v. 31, p. 917–920.
- JIANG, G., CHRISTIE-BLICK, N., KAUFMAN, A.J., BANERJEE, D.M., AND RAI, V., 2003c, Carbonate platform growth and cyclicity at a terminal Proterozoic passive margin, Infra Krol Formation and Krol Group, Lesser Himalaya, India: *Sedimentology*, v. 50, p. 921–952.
- KATZ, M.E., PAK, D.K., DICKENS, G.R., AND MILLER, K.G., 1999, The Source and fate of massive carbon input during the latest Paleocene thermal maximum: *Science*, v. 286, p. 1531–1533.
- KAUFFMAN, E.G., ARTHUR, M.A., HOWE, B., AND SCHOLLE, P.A., 1996, Widespread venting of methane-rich fluids in Late Cretaceous (Campanian) submarine springs (Tepee Buttes), Western Interior Seaway, U.S.A.: *Geology*, v. 24, p. 799–802.
- KAUFMAN, A.J., KNOLL, A.H., AND NARBONNE, G.M., 1997, Isotopes, ice ages, and terminal Proterozoic earth history: U.S. National Academy of Sciences, *Proceedings*, v. 94, p. 6600–6605.
- KELLY, S.R.A., DITCHFIELD, P.W., DOUBLEDAY, P.A., AND MARSHALL, J.D., 1995, An Upper Jurassic methane-seep limestone from the Fossil Bluff Group forearc basin of Alexander Island, Antarctica: *Journal of Sedimentary Research*, v. 65, p. 274–282.
- KENDALL, A.C., 1985, Radial fibrous calcite: a reappraisal, in Schneidermann, N., and Harris, P.M., eds., *Carbonate Cements: SEPM, Special Publication 36*, p. 59–77.
- KENDALL, A.C., AND TUCKER, M.E., 1973, Radial fibrous calcite: a replacement after acicular carbonate: *Sedimentology*, v. 20, p. 365–389.
- KENDALL, C.G.St.C., AND WARREN, J., 1987, A review of the origin and setting of tepees and their associated fabrics: *Sedimentology*, v. 34, p. 1007–1027.
- KENNEDY, M.J., 1996, Stratigraphy, sedimentology, and isotopic geochemistry of Australian Neoproterozoic postglacial cap dolostones: deglaciation, $\delta^{13}\text{C}$ excursions, and carbonate precipitation: *Journal of Sedimentary Research*, v. 66, p. 1050–1064.
- KENNEDY, M.J., RUNNEGAR, B., PRAVE, A.R., HOFFMANN, K.H., AND ARTHUR, M.A., 1998, Two or four Neoproterozoic glaciations?: *Geology*, v. 26, p. 1059–1063.
- KENNEDY, M.J., CHRISTIE-BLICK, N., AND SOHL, L.E., 2001, Are Proterozoic cap carbonates and isotopic excursions a record of gas hydrate destabilization following Earth's coldest intervals?: *Geology*, v. 29, p. 443–446.
- KNOLL, A.H., AND HOLLAND, H.D., 1995, Oxygen and Proterozoic evolution: an update, in Stanley, S.M., ed., *Effects of Past Global Change on Life*: Washington, DC, National Academy Press, p. 21–33.
- KNOLL, A.H., BAMBACH, R.K., CANFIELD, D.E., AND GROTZINGER, J.P., 1996, Comparative Earth history and Late Permian mass extinction: *Science*, v. 273, p. 452–457.
- KULM, L.D., AND SUESS, E., 1990, Relationship between carbonate deposits and fluid venting: Oregon accretionary prism: *Journal of Geophysical Research*, v. 95, p. 8899–8915.
- KVENVOLDEN, K.A., 1988, Methane hydrate: a major reservoir of carbon in the shallow geosphere?: *Chemical Geology*, v. 71, p. 41–51.
- KVENVOLDEN, K.A., 1998, A primer on the geological occurrence of gas hydrate, in Henriet, J.-P., and Mienert, J., eds., *Gas Hydrate: Relevance to World Margin Stability and Climate Change*: Geological Society of London, Special Publication 137, p. 9–30.
- KVENVOLDEN, K.A., 2002, Methane hydrate in the global organic carbon cycle: *Terra Nova*, v. 14, p. 302–306.
- LEATHER, J., ALLEN, P.A., BRASIER, M.D., AND COZZI, A., 2002, Neoproterozoic snowball Earth under scrutiny: evidence from the Fiq Glaciation of Oman: *Geology*, v. 30, p. 891–894.
- LI, Z.X., LI, X.H., KINNY, P.D., AND WANG, J., 1999, The breakup of Rodinia: did it start with a mantle plume beneath South China?: *Earth and Planetary Science Letters*, v. 173, p. 171–181.
- LING, W., GAO, S., ZHANG, B., LI, H., LIU, Y., CHENG, J., CHO, M., AND LI, X., 2003, Neoproterozoic tectonic evolution of the northwestern Yangtze Craton, South China: implications for amalgamation and break-up of the Rodinia supercontinent: *Precambrian Research*, v. 122, p. 111–140.
- LIU, B., XU, X., PAN, X., HUANG, H., AND XU, Q., 1993, Paleoclimatic Sediments, Crust Evolution and Ore Deposits of South China: Beijing, Science Press, 236 p.
- LIU, H., et al., 1991, The Sinian System in China: Beijing, Science Press, 387 p.
- MA, G., LEE, H., AND ZHANG, Z., 1984, An investigation of the age limits of the Sinian System in south China: Yichang Institute of Geology and Mineral Resources, *Bulletin*, v. 8, p. 1–29.
- MACDONALD, I.R., SAGER, W.W., AND PECCINI, M.B., 2003, Gas hydrate and chemosynthetic biota in mounded bathymetry at mid-slope hydrocarbon seeps: Northern Gulf of Mexico: *Marine Geology*, v. 198, p. 133–158.
- MOORE, C.H., 1989, Carbonate diagenesis and porosity: Amsterdam, Elsevier, 338 p.
- NOGUEIRA, A.C.R., RICCOMINI, C., SIAL, A.N., MOURA, C.A.V., AND FAIRCHILD, T.R., 2003, Soft-sediment deformation at the base of the Neoproterozoic Puga cap carbonate (southwestern Amazon craton, Brazil): Confirmation of rapid icehouse to greenhouse transition in snowball Earth: *Geology*, v. 31, p. 613–616.
- PECKMANN, J., AND THIEL, V., 2004, Carbon cycling at ancient methane-seeps: *Chemical Geology*, v. 205, p. 443–467.
- PECKMANN, J., GOEDERT, J.L., THIEL, V., MICHAELIS, W., AND REITNER, J., 2002, A comprehensive approach to the study of methane-seep deposits from the Lincoln Creek Formation, western Washington State, USA: *Sedimentology*, v. 49, p. 855–873.
- PLUMMER, P.S., 1978, Note on the paleoenvironmental significance of the Nuccaleena Formation (upper Precambrian), central Fingers Ranges, South Australia: *Geological Society of Australia, Journal*, v. 25, p. 395–402.
- PORTER, S.M., KNOLL, A.H., AND AFFATON, P., 2004, Chemostratigraphy of Neoproterozoic cap carbonates from the Volta Basin, West Africa: *Precambrian Research*, v. 130, p. 99–112.
- QIAO, X.F., 1989, Southeast China region, *Stratigraphy of China (3)*: Beijing, Geological Publishing House, p. 261–267.
- RIDGWELL, A.J., AND KENNEDY, M.J., 2004, Secular changes in the importance of neritic carbonate deposition as a control on the magnitude and stability of Neoproterozoic ice ages, in Jenkins, G.S., McMenamin, M., McKay, C.P., and Sohl, L.E., eds., *Multidisciplinary Studies Exploring Extreme Proterozoic Environment Conditions*: American Geophysical Union, *Geophysical Monographs Series*, v. 146, p. 55–72.
- RIDGWELL, A.J., KENNEDY, M.J., AND CALDEIRA, K., 2003, Carbonate deposition, climate stability, and Neoproterozoic ice ages: *Science*, v. 302, p. 859–862.
- RUNNEGAR, B., 2000, Loophole for snowball Earth: *Nature*, v. 405, p. 403–404.
- SANDBERG, P., 1985, Aragonite cements and their occurrence in ancient limestones, in Schneidermann, N., and Harris, P.M., eds., *Carbonate Cements: SEPM, Special Publication 36*, p. 33–57.
- SAVARD, M.M., BEAUCHAMP, B., AND VEIZER, J., 1996, Significance of aragonite cements around Cretaceous marine methane seeps: *Journal of Sedimentary Research*, v. 66, p. 430–438.
- SAYLOR, B.Z., GROTZINGER, J.P., AND GERMS, G.J.B., 1995, Sequence stratigraphy and sedimentology of the Neoproterozoic Kuibis and Schwarzrand subgroups (Nama Group), southwestern Namibia: *Precambrian Research*, v. 73, p. 153–171.
- SHIELDS, G.A., 2005, Neoproterozoic cap carbonates: a critical appraisal of existing models and the plume world hypothesis: *Terra Nova*, v. 17, p. 299–310.
- SIEDLECKA, A., AND ROBERTS, D., 1992, The Bedrock Geology of Varanger Peninsula, Finnmark, North Norway: An Excursion Guide, Geological Survey of Norway, 45 p.
- STAKES, D.S., ORANGE, D.L., PADUAN, J.B., SALAMY, K.A., AND MAHER, N., 1999, Cold-seeps and authigenic carbonate formation in Monterey Bay, California: *Marine Geology*, v. 159, p. 93–109.
- STEINER, M., MEHL, D., REITNER, J., AND ERDTMANN, B.-D., 1993, Oldest entirely preserved sponges and other fossils from the lowermost Cambrian and a new facies reconstruction of the Yangtze platform (China): *Berliner Geowissenschaftliche Abhandlungen (E)*, v. 9, p. 293–329.

- Suess, E., Torres, M.E., Bohrmann, G., Collier, R.W., Greinert, J., Linke, P., Rehder, G., Trehu, A., Wallmann, K., Winckler, G., and Zuleger, E., 1999, Gas hydrate destabilization: enhanced dewatering, benthic material turnover and large methane plumes at the Cascadia convergent margin: *Earth and Planetary Science Letters*, v. 170, p. 1–15.
- Suess, E., Torres, M.E., Bohrmann, G., Collier, R.W., Rickert, D., Goldfinger, C., Linke, P., Heuser, A., Sahlng, H., Heeschen, K., Jung, C., Nakamura, K., Greinert, J., Pfannkuche, O., Trehu, A., Linkhammer, G., Whiticar, M.J., Einsenhauer, A., Teichert, B., and Elvert, M., 2001, Sea floor methane hydrates at Hydrate Ridge, Cascadia margin, in Dillon, W.P., and Paull, C.K., eds., *Natural Gas Hydrates: Occurrence, Distribution and Dynamics*: American Geophysical Union, Geophysical Monograph Series, v. 124, p. 87–98.
- Sun, W.G., 1986, Late Precambrian pennatulids (sea pens) from the eastern Yangtze Gorge: *Paracharnia* gen. nov.: *Precambrian Research*, v. 31, p. 361–375.
- Torres, M.E., McManus, J., Hammond, D.E., De Angelis, M.A., Heeschen, K.U., Colbert, S.L., Tryon, M.D., Brown, K.M., and Suess, E., 2002, Fluid and chemical fluxes in and out of sediments hosting methane hydrate deposits on Hydrate Ridge, OR; I. Hydrological provinces: *Earth and Planetary Science Letters*, v. 201, p. 525–540.
- Torres, M.E., Bohrmann, G., Dube, T.E., and Poole, F.G., 2003, Formation of modern and Paleozoic stratiform barite at cold methane seeps on continental margins: *Geology*, v. 31, p. 897–900.
- Torres, M.E., Wallmann, K., Trehu, A.M., Bohrmann, G., Borowski, W.S., and Tomaru, H., 2004, Gas hydrate growth, methane transport, and chloride enrichment at the southern summit of Hydrate Ridge, Cascadia margin off Oregon: *Earth and Planetary Science Letters*, v. 226, p. 225–241.
- Tryon, M.D., Brown, K.M., and Torres, M.E., 2002, Fluid and chemical flux in and out of sediments hosting methane hydrate deposits on Hydrate Ridge, OR, II: Hydrological processes: *Earth and Planetary Science Letters*, v. 201, p. 541–557.
- Tucker, M.E., Wright, V.P., and Dickson, J.A.D., 1990, *Carbonate Sedimentology*: London, Blackwell Scientific Publications, 482 p.
- Van Dover, C.L., Aharon, P., Bernhard, J.M., Caylor, E., Doerries, M., Flickinger, W., Gilhooly, W., Goffredi, S.K., Knick, K.E., Macko, S.A., Rapoport, S., Raulfs, E.C., Ruppel, C., Salerno, J.L., Seitz, R.D., Gupta, B.K.S., Shank, T., Turnipseed, M., and Vrijenhoek, R., 2003, Blake Ridge methane seeps; characterization of a soft-sediment, chemosynthetically based ecosystem: *Deep-Sea Research I*, v. 50, p. 281–300.
- Wallace, M.W., 1987, The role of internal erosion and sedimentation in the formation of stromatolite mudstones and associated lithologies: *Journal of Sedimentary Petrology*, v. 57, p. 695–700.
- Walter, M.R., and Bauld, J., 1983, The association of sulphate evaporites, stromatolite carbonates and glacial sediments: examples from the Proterozoic of Australia and the Cainozoic of Antarctica: *Precambrian Research*, v. 21, p. 129–148.
- Wang, H.Z., et al., 1985, *Atlas of the Paleogeography of China*: Beijing, Cartographic Publishing House, 143 p.
- Wang, J., and Li, Z.-X., 2003, History of Neoproterozoic rift basins in South China; implications for Rodinia break-up: *Precambrian Research*, v. 122, p. 141–158.
- Wang, X., Erdtmann, B.-D., Chen, X., and Mao, X., 1998, Integrated sequence-, bio- and chemostratigraphy of the terminal Proterozoic to lowest Cambrian “black rock series” from central South China: *Episodes*, v. 21, p. 178–189.
- Wang, Y., Lu, S., Gao, Z., Lin, W., and Ma, G., 1981, Sinian tillites of China, in Hambrey, M.J., and Harland, W.B., eds., *Earth's Pre-Pleistocene Glacial Record*: Cambridge, U.K., Cambridge University Press, p. 386–401.
- Williams, G.E., 1979, Sedimentology, stable isotope geochemistry and paleoenvironment of dolostones capping late Precambrian glacial sequences in Australia: *Geological Society of Australia, Journal*, v. 26, p. 377–386.
- Xiao, S., 2004, New multicellular algal fossils and acritarchs in Doushantuo chert nodules (Neoproterozoic; Yangtze Gorge area, south China): *Journal of Paleontology*, v. 78, p. 393–401.
- Xiao, S., Yun, Z., and Knoll, A.H., 1998, Three-dimensional preservation of algae and animal embryos in a Neoproterozoic phosphorite: *Nature*, v. 391, p. 553–558.
- Xiao, S., Bao, H., Wang, H., Kaufman, A.J., Zhou, C., Li, G., Yuan, X., and Ling, H., 2004, The Neoproterozoic Quruqtagh Group in eastern Chinese Tianshan: evidence for a post-Marinoan glaciation: *Precambrian Research*, v. 130, p. 1–26.
- Xiao, S., Shen, B., Zhou, C., Xie, G., and Yuan, X., 2005, A uniquely preserved Ediacaran fossil with direct evidence for a quilted bodyplan: *U.S. National Academy of Sciences, Proceedings*, v. 102, p. 10,227–10,232.
- Yin, A., and Nie, S.Y., 1996, A Phanerozoic palinspastic reconstruction of China, in Yin, A., and Harrison, T.M., eds., *The Tectonic Evolution of Asia*: Cambridge, U.K., Cambridge University Press, p. 442–485.
- Yin, C., 1999, Microfossils from the Upper Sinian (late Neoproterozoic) Doushantuo Formation in Changyang, western Hubei, China: *Continental Dynamics*, v. 4, p. 1–18.
- Yin, C., Liu, D., Gao, L., Wang, Z., Xing, Y., Jian, P., Shi, Y., and Anonymous, 2003, Lower boundary age of the Nanhua System and the Gucheng glacial stage; evidence from SHRIMP II dating: *Chinese Science Bulletin*, v. 48, p. 1657–1662.
- Yin, C., Bengtson, S., and Yue, Z., 2004, Silicified and phosphatized Tianzhusania, spheroidal microfossils of possible animal origin from the Neoproterozoic of South China: *Acta Palaeontologica Polonica*, v. 49, p. 1–12.
- Zhang, S., Jiang, G., Zhang, J., Song, B., Kennedy, M.J., and Christie-Blick, N., 2005, U–Pb sensitive high-resolution ion microprobe ages from the Doushantuo Formation in south China: Constraints on late Neoproterozoic glaciations: *Geology*, v. 33, p. 473–476.
- Zhang, T., Chu, X., Zhang Qi, R., Feng, L., and Huo, W., 2003, Variations of sulfur and carbon isotopes in seawater during the Doushantuo stage in late Neoproterozoic: *Chinese Science Bulletin*, v. 48, p. 1375–1380.
- Zhang, Y., Yin, L., Xiao, S., and Knoll, A.H., 1998, Permineralized fossils from the terminal Proterozoic Doushantuo Formation, south China: *The Paleontological Society, Memoir* 50, p. 1–52.
- Zhao, Z., Xing, Y., Ma, G., and Chen, Y., 1985, *Biostratigraphy of the Yangtze Gorge area, (1) Sinian*: Beijing, Geological Publishing House, 143 p.
- Zhao, Z., Xing, Y., Ding, Q., Liu, G., Zhao, Y., Zhang, S., Meng, X., Yin, C., Ning, B., and Han, P., 1988, *The Sinian System of Hubei*: Wuhan, China University of Geosciences Press, 205 p.
- Zheng, Y., 2003, Neoproterozoic magmatic activity and global change: *Chinese Science Bulletin*, v. 48, p. 1639–1656.
- Zheng, Y., Wu, Y., Chen, F., Gong, B., Li, L., and Zhao, Z., 2004, Zircon U–Pb and oxygen isotope evidence for a large-scale ¹⁸O depletion event in igneous rocks during the Neoproterozoic: *Geochimica et Cosmochimica Acta*, v. 68, p. 4145–4165.
- Zhou, C., Yan, K., Hu, J., Meng, F., Cheng, Z., Xue, Y., Bao, H., and Yuan, X., 2001, The Neoproterozoic tillites at Lantian, Xiuning County, Anhui Province: *Journal of Stratigraphy*, v. 25, p. 247–252.
- Zhou, C., Tucker, R., Xiao, S., Peng, Z., Yuan, X., and Chen, Z., 2004, New constraints on the ages of Neoproterozoic glaciations in south China: *Geology*, v. 32, p. 437–440.

Received 28 April 2005; accepted 25 January 2006.